P-T evolution of paragneisses and amphibolites from Romeleåsen, Scania, southernmost Sweden

Jan Ulmius

Dissertations in Geology at Lund University,
Master's thesis, no 327
(45 hp/ECTS credits)

Department of Geology
Lund University
2013

P-T evolution of paragneisses and amphibolites from Romeleåsen, Scania, southernmost Sweden

Master's thesis

Jan Ulmius

Department of Geology
Lund University
2013

Contents

Cover Picture: Outcrop on Romeleklint with garnet porphyroblasts most likely representing a melt. Photo: Jan Ulmius

P-T evolution of paragneisses and amphibolites from Romelåsen, Scania, southernmost Sweden

JAN ULMIUS

Ulmius, J., 2013: P-T evolution of paragneisses and amphibolites from Romeleåsen, Scania, southernmost Sweden. *Dissertations in Geology at Lund University*, No. 327, 34 pp. 45 hp (45 ECTS credits) .

Abstract: Romeleåsen is the south-westernmost exposure of the Fennoscandian Shield in Sweden. Fennoscandia forms a part of the East European Craton and was extended to the south-west during prolonged episodes of accretion during the period 1.95-1.55 Ga. Metamorphic reworking took at least place during the Hallandian/ Danopolonian orogeny at 1.47-1.38 Ga and during the Sveconorwegian orogeny 1.10-0.92 Ga. High-grade metamorphism during the Sveconorwegian orogeny may have overprinted Hallandian/Danopolonian metamorphism fully or only in parts of Romeleåsen. Alternatively is high-grade metamorphism pre-Sveconorwegian and Sveconorwegian metamorphism caused only a retrograde overprint.

Petrographic and geochemical studies including geothermobarometry and calculation of pseudosections on paragneisses and amphibolites from the middle part of Romeleåsen were performed with the aim of understanding the metamorphism.

The results show that rocks of the middle part of Romeleåsen underwent prograde staurolite-sillimanite grade metamorphism at upper amphibolite to granulite conditions peaking at about 750°C and 4-5 kbar, with formation of Crd + Sill + Grt + Kfs + Ilm + Melt ± Spl ± Bt. A clockwise P-T path is proposed with heating during decompression and partial melting. Later stages involved the formation of sillimanite + biotite at the expense of garnet and cordierite. Local low-temperature and fluid-assisted retrogression caused pseudomorphism of cordierite by muscovite, biotite and chlorite. Also pseudomorphism of ilmenite by rutile-rich fine-grained intergrowths can be observed.

The P-T evolution demonstrates burial and exhumation in a high T/P environment, probably due to coeval magmatism. These conditions are in accordance with an accretionary orogenic setting.

In order to assign the metamorphism to either the Hallandian/Danopolonian or the Sveconorwegian orogeny, geochronological studies could be performed, as a suggestion on the abundant zircons in the paragneisses.

Keywords: Romeleåsen, metamorphism, geothermobarometry, pseudosection, Theriak-Domino, P-T path, Hallandian/Danopolonian, Sveconorwegian

Supervisors: Charlotte Möller, Leif Johansson

Subject: Lithosphere and Paleobiosphere Sciences

Jan Ulmius, Department of Geology, Lund University, Sölvegatan 12, SE-223 62 Lund, Sweden.
E-mail: jan.ulmius@telia.com

Tryck-temperatur utveckling för paragnejser och amfiboliter från Romeleåsen, Skåne

JAN ULMIUS

Ulmius, J., 2013: Tryck-temperatur utveckling för paragnejser och amfiboliter från Romeleåsen, Skåne. *Examensarbeten i geologi vid Lunds universitet*, Nr. 327, 34 sid. 45 hp.

Sammanfattning: Romeleåsen är den sydvästligaste blottningen av den Fennoskandiska skölden i Sverige. Fennoskandia som är en del av Östeuropakratonen utökades mot sydväst vid långvariga tillväxtepisoder under perioden 1.95-1.55 miljarder år. Berggrunden har påverkats metamorfiskt åtminstone under den hallandiska/danopoloniska orogenesen för 1.47-1.38 miljarder år sedan och under den svekonorvegiska orogenesen för 1.10-0.92 miljarder år sedan. Höggradig metamorfism under den svekonorvegiska orogenesen kan ha förstört tecknen på hallandisk/danopolonisk metamorfism helt eller endast i delar av Romeleåsen. Ett annat alternativ är att den höggradiga metamorfismen är pre-svekonorvegisk och att svekonorvegisk metamorphism endast orsakade ett retrograd övertryck.

För att försöka förstå metamorfismen har petrografin och geokemin studerats för paragnejser och amfiboliter från Romeleåsens mellersta del. Geotermobarometri och pseudosektioner har använts för att sätta en mer kvantitativ siffra på P-T-utvecklingen.

Resultatet visar att berget i mellersta delen av Romeleåsen gick igenom en prograd staurolit-sillimanit metamorfism vid övre amfibolit till granulit betingelser med maximum vid cirka 750°C och 4-5 kbar. Paragenesen kan beskrivas med Crd + Sill + Grt + Kfs + Ilm + Melt ± Spl ± Bt. Tryck och temperatur följer en bana medurs med uppvärmning under trycksänkning och partiell smältning. Senare stadier involverar bildning av sillimanit + biotit på bekostnad av granat och kordierit. Pseudomorfer med muskovit, biotit och klorit har bildats av kordierit vid låg temperatur under medverkan av en flytande fas. Pseudomorfer med finkornig rutil efter ilmenit kan också observeras.

Tryck-temperatur utvecklingen tyder på berg som begravts och sedan lyfts upp. Detta har skett i en omgivning med högt temperatur/tryck förhållande, vilket tyder på samtidig magmatism. Betingelserna är i samklang med orogener som bildas i subduktionszoner.

För att kunna hänföra metamorfismen till hallandisk/danopolonisk eller svekonorvegisk behövs geokronologiska studier. Ett lämpligt mineral är zirkon, som finns talrikt i paragnejserna på Romeleåsen.

Nyckelord: Romeleåsen, metamorfism, geotermobarometri, pseudosektion, Theriak-Domino, P-T-utveckling, halandisk/danopolonisk, svekonorvegisk

Jan Ulmius, Geologiska institutionen, Lunds universitet, Sölvegatan 12, 223 62 Lund, Sverige.
E-post: jan.ulmius@telia.com

1 Introduction

Romeleåsen is the south-westernmost exposure of the Fennoscandian Shield in Sweden (Fig. 1). Fennoscandia forms a part of the East European Craton and was extended to the south-west during prolonged episodes of accretion: the Svecofennian orogeny at 1.95-1.85 Ga, the Trans-Scandinavian Igneous belt (TIB) continental margin magmatism at 1.86-1.65 Ga and the Gothian orogeny at 1.73-1.55 Ga (Bogdanova et al. 2008; Högdahl et al. 2004; Brueckner 2009; Appelquist 2010 and references therein). Metamorphic reworking took place during the Hallandian-/Danopolian orogeny at 1.47-1.38 Ga (Brander 2011) and references therein), and during the Sveconorwegian orogeny 1.10-0.92 Ga (Bingen et al. 2008b and references therein).

It has been proposed (Brander 2011) that the Hallandian/Danopolian orogeny was caused by collision between Fennoscandia and an unknown continent in the southwest at 1.45-1.42 Ga, leaving an E-W to NW-SE trending gneissic fabric on Bornholm, Scania, Blekinge and also further north. This was largely overprinted by the Sveconorwegian orogeny in the Eastern Segment (Fig. 1) at 0.98-0.97 Ga (Möller et al. 2007; Bingen et al. 2008a).

The P-T conditions, P-T evolution and age of the metamorphism at Romeleåsen are still not fully known although Hjelmqvist (1934) estimated the conditions to >600°C and 5-6 kbar, i.e. amphibolite facies. It is possible that the westernmost part was affected by the Sveconorwegian orogeny resulting in high-grade metamorphism (and the formation of garnet amphibolites and high-P granulites) and that the eastern part was only weakly affected by this orogeny, and instead shows traces of pre-Sveconorwegian metamorphism (i.e. Hallandian/Danopolonian metamorphism). Another possibility is that the high-grade metamorphism is pre-Sveconorwegian in age and that Sveconorwegian metamorphism caused a retrograde overprint. Recent dating of metadolerite dykes along the Romeleåsen shows a predominant Sveconorwegian metamorphic disturbance of baddeleyite, albeit decreasing to the east (Cederberg 2011).

1.1 Objectives

This project aims at characterization of the metamorphism in the Romeleåsen horst including determination of the peak P-T conditions and P-T path of selected rocks, using in the first place cordierite-, garnet- and Al-silicate-bearing parageneses and their textural relations, microgeochemistry and geothermobarometry, whole-rock chemical analysis and thermodynamic calculations (pseudosections).

2 Geological setting and general petrography

The south-western Fennoscandian Shield was affected by the Caledonian orogeny during Early Silurian, leading to faulting and horst and graben structures along the Tornquist zone (Erlström et al. 1997). During Mesozoic and Tertiary compression, the horst Romeleåsen (Fig. 2) was raised by fault reactivation in the Tornqvist zone (Bergerat et al. 2007). On the horst, crystalline rocks are exposed in a limited number of outcrop areas and quarries. The dominating rocks are red to greyish red gneisses, which probable are of magmatic origin (Erlström et al. 2004). One dating of a gneiss from Stenberget suggests a protolith age of 1.65-1.7 Ga (Johansson et al. 1993), which falls in the range of TIB rocks. The gneisses are fine-grained and generally leucocratic with a more or less pronounced

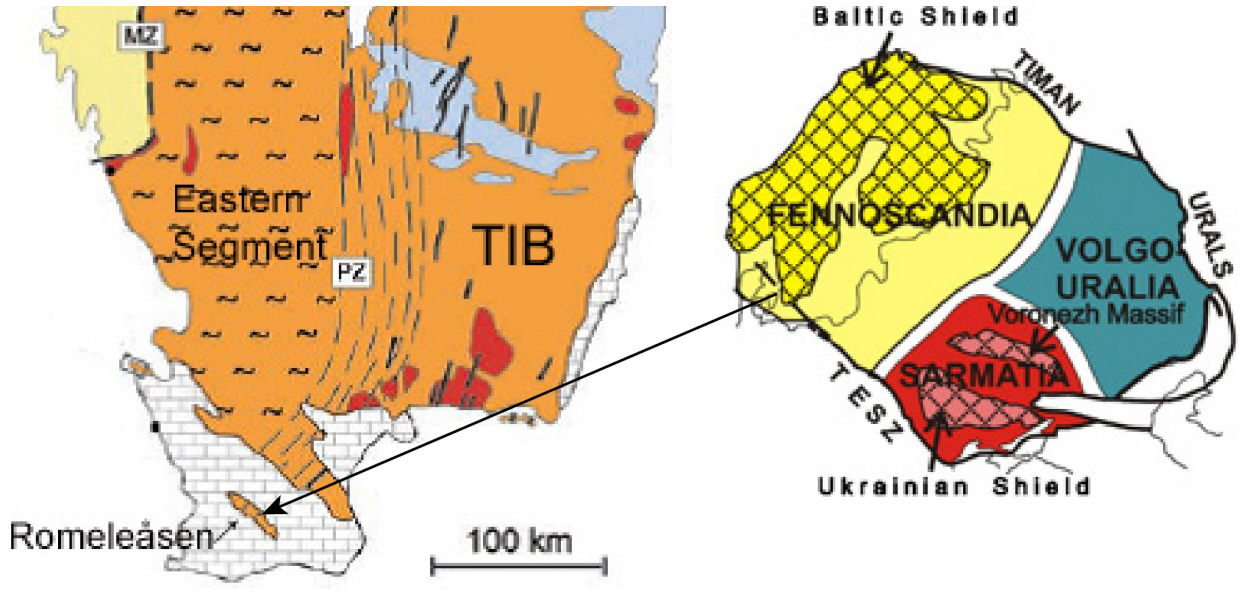

Fig. 1. Simplified geological map of southern Sweden (left: modified from Söderlund et al. 2008, fig. 1) and the relation of the Fennoscandian Shield to the East European Craton (right: modified from Bogdanova et al. 2008, fig. 1).

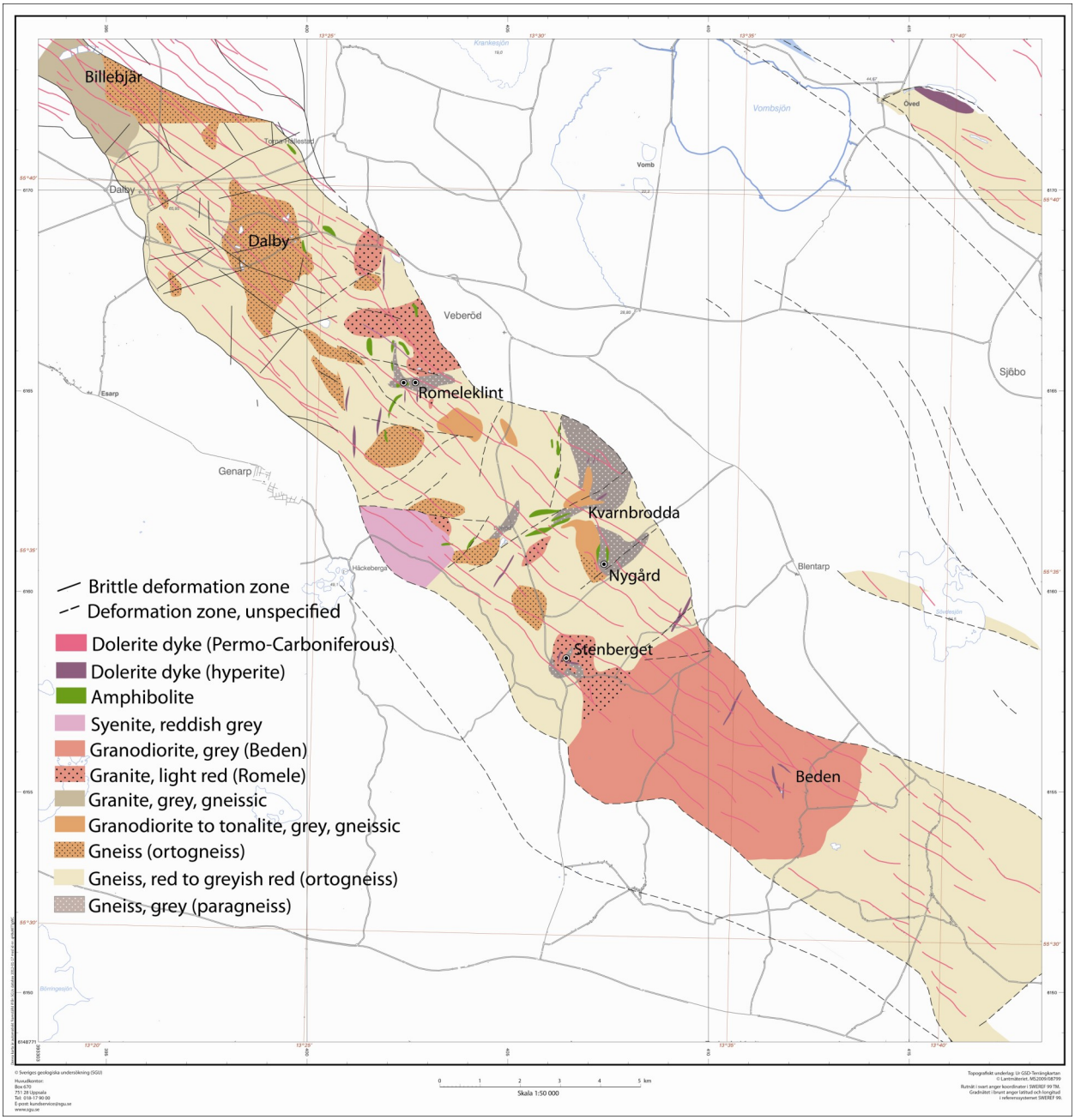

Fig. 2. Geological map of Romeleåsen (background map source SGU 2012 modified with data from printed maps (Erlström et al. 2012, Erlström et al. 2001 and Erlström et al. 1998).

foliation. The composition varies but the main minerals are quartz, perthitic microcline and plagioclase with a few percent biotite and other dark minerals (Hjelmqvist 1934).

In the mid-part of Romeleåsen, in the areas Romeleklint, Dörröd, Kvarnbrodda, Nygård and Stenberget, aluminous greyish gneiss varieties containing sillimanite, cordierite and/or garnet are present. They have been interpreted as supracrustal in origin (paragneisses), either volcanic or sedimentary (Hjelmqvist 1934). Hjelmqvist used the term "leptite gneiss" for paragneisses of presumed volcanic origin, usually fine-grained grey or grey-red rocks and commonly banded. They are granoblastic and dominated by quartz, microcline, and plagioclase; with up to 10% biotite, and small amounts of garnet, muscovite, and opaques. Among paragneisses of presumed sedimentary origin Hjelmqvist discerned quartz phyllite, cordierite-sillimanite gneiss, garnet-muscovite gneiss, and garnet-biotite gneiss. Cordierite-sillimanite gneiss can be found at all above mentioned localities; this rock is often fine-grained with blue-grey specks. The specks are pseudomorphs after cordierite, formed during retrogression with formation of biotite-sillimanite aggregates at higher temperatures and fine-grained muscovite or talc (pinitisation) at lower temperatures. The cordierite-sillmanite gneiss is variably deformed, in some sites it is granoblastic, in other sites it is banded

or foliated. Partial melting can also be observed. Hjelmqvist (1934) summarised the paragenesis as Qtz + Kfs + Pl + Bt + Sil + Ms + Grt + Opq ± Crd ± Spl ±Zrn ±Ap where most of the biotite, sillimanite and muscovite occur in pseudomorphs after cordierite. Hjelmqvist also report exceptional findings of andalusite.

Concentrated in the mid-north part of Romeleåsen are layers and slivers of amphibolite, which occur concordant with the gneisses and are therefore probably close in age and origin. Other amphibolitic dykes cut the gneissic structures and are younger (Erlström et al. 2004). Hjelmqvist (1934) differentiated a number of amphibolite types: cummingtonite amphibolite, hypersthene amphibolite, anthophyllite amphibolite and quartz amphibolite.

Locally, young "granites" can be found, e.g. the reddish "Romele granite" at Veberöd, Stenberget, Nygård and north of Romeleklint and the greyish "Beden granite" (granodiorite with hornblende and pyroxenes) in the Beden area. The "Beden granite" has been dated at 1449^{+23}_{-11} Ma (Johansson et al. 1993), which corresponds to the age of Karlshamn and Spinkamåla granits further east in Blekinge. The "Romele granite" was considered likely to be of the same age by Erlström et al. (2004); unpublished zircon dating (J. Andersson) has confirmed this interpretation. These granites show weak deformation (Hjelmqvist 1934). Another young intrusive rock is the greenish grey to reddish grey Billebjär gneiss-granite from the northwestern tip of the Romeleåsen, homogeneous in appearance and containing hornblende and probably altered pyroxenes. It has been proposed that this rock has undergone charnockitisation (Sivhed et al. 1999).

Hjelmqvist (1934) noted that the strike of the gneissosity and compositional banding in the northwestern part of Romeleåsen is consistently N-S to NW -SO, However further south-east the picture is more unclear, and the strike changes from E-W over N-S to NO-SW. The dip of the gneissosity or banding is steep, usually >60°. Observed folding with gently (20-30°) plunging fold axes is likely the result of compression in E-W to NE-SW direction (Hjelmqvist 1934).

A set of NNE-SSW-oriented dykes of black dolerite ("hyperite") is concentrated to the mid-north part of Romeleåsen. The dolerites are fine- to medium-grained and black to brownish violet. The texture is ophitic to subophitic with plagioclase laths and augitic pyroxene grains partly altered to hornblende. Some of the dykes have recently been dated using U-Pb dating of baddeleyite (Cederberg 2011). Dolerite dykes in quarries at Dalby and Veberöd yielded minimum ages of 1166±16 and 1242±28 Ma, respectively, while a dolerite in a dyke in a quarry at Beden gave a minium age of 1238±10 Ma. The dykes at Dalby and Veberöd therefore appear to be of the same generation as the dykes identified within the so called Protogine Zone (PZ, Fig. 1), in the easternmost parts of the Sveconorwegian Province. The dykes originally intruded into rocks of the Transscandinavian Ignous Belt.

Finally, Romeleåsen was intruded by a set of numerous, steeply dipping dolerite dykes running NW-SE to WEW-ESE during the Carboniferous and Permian (Erlström et al. 2004).

3 Methods

Samples sites were selected using information from Hjelmquist (1934) and Erlström et al. (1997). Out of about 60 rock samples from Romeleåsen, 40 thin sections were prepared and investigated by polarised light microscopy. Ten thin sections were carbon coated and investigated by scanning electron microscopy (SEM) using a Hitachi S-3400N fitted with an EDS analyser (Oxford Instruments with INCA software) for quantitative analysis. An acceleration voltage of 15 kV at a working distance of 10 mm was used. Quant optimisation was performed frequently using a Co-standard with the aim of keeping within 99-101% of preceding measurement. Quantifying was performed with a livetime of 60-80 seconds against natural and synthetic standards. The aim was that total elements for hydrogen-free minerals should be within 99-101% and for hydrogen-bearing minerals within 93-97%. Line-scans were performed on garnets and other minerals used in the calculations to verify any zonation.

Major elements were analysed by inductively coupled plasma emission spectroscopy (ICP) on rock pulp from the same samples used for preparing thin sections.

Quantitative P-T conditions were evaluated using the program winTWQ (version 2.34) (Berman 2007) (Berman 1991) based on the internally consistent thermodynamic dataset of Berman (1988) (Berman & Aranovich 1996). TWQ uses a multi-equilibrium approach with P and T determined from the intersection of independent reactions in P-T space.

In samples where aluminosilicates (e.g. sillimanite) were absent, the calibrated garnet-biotite-plagioclase-quartz (GBPQ) by Wu et al. (2004) was used. It is suitable under the conditions 515-878°C, 1.0-11.4 kbar, X_{Gr}>3%, X_{An}>17% and X_{Al}^{Bt}>3% in medium to high-grade metapelites.

As an independent test the Ti-in-biotite geothermometer by Henry et al. (2005) was used. This is suitable to use in graphitic peraluminous metapelites, which contain quartz and ilmenite or rutile and have equilibrated at roughly 3-6 kbar. For optimum performance the Mg/(Mg+Fe), Ti and temperature should be in the range 0.275-1.0, 0.04-0.6 apfu and 480-800°C, respectively.

For amphibolites the Hbl-Pl geothermometer by Holland & Blundy (1994) and the geobarometer by Lawford Anderson & Smith (1995) were used.

Equilibrium phase diagrams using the analysed bulk rock compositions were calculated in the system MnNCKFMASHT using the software THERIAK-DOMINO version 03.01.2012 (de Capitani & Petrakakis 2010; de Capitani 2012) with the thermodynamic database of Holland & Powell (1998) updated to da-

taset 5.5 (tc-ds55, Powell & Holland 2012). Solution models used for different minerals are according to Appendix 1. Other phases and H_2O are considered as pure end-member phases. As P is not included in the modelling the CaO of apatite was subtracted from the total CaO of the rock. The P-T pseudosections use a quantity of H_2O just sufficient to saturate the solidus at a pressure of 5-7 kbar and are mainly appropriate for a prograde evolution. Melt proportions are therefore overestimated for P-T paths that cross the solidus at lower pressure. The bulk composition formula Fe_2O_3 is calculated as Fe^{2+}. THERIAK-DOMINO is not well documented for calculation with Fe^{3+} which was therefore not included in the solution models.

4 Results

4.1 Sample sites and samples

Sample sites investigated in this study are Romeleklint, Nygård and Stenberget (Fig. 2). Romeleklint is the highest point on Romeleåsen (175 m above sea level) and has been geologically mapped in detail by Hjelmqvist (1934), see Fig. 3. The largest, western outcrop consists mainly of amphibolite transected by dolerite dykes (by Hjelmqvist termed hyperite diabase). Two smaller outcrops with paragneisses to the west of the amphibolite outcrop do not exist any longer (a telecommunications tower has been built on the outcrops). The large eastern outcrop contains both paragneiss and amphibolite. The Nygård outcrop (about 30 m in diameter) consists solely of spotted grey gneiss. Stenberget is an active quarry where mainly light red granite is quarried; however, in the eastern wall paragneisses of different appearances are present. Samples used in this study are presented in Table 1.

The rock types investigated in this study are garnet -sillimanite-biotite gneisses (leptite gneiss, cordierite-sillimanite gneiss or garnet-biotite gneiss according to Hjelmqvist; paragneisses containing cordierite pseudomorphs (cordierite-sillimanite gneiss of Hjelmqvist); garnet-sillimanite-muscovite-biotite gneisses (likely with pseudomorphs after cordierite); and amphibolites.

4.2 Bulk-rock chemistry

Bulk-rock analyses of hand specimens (remains from the thin section preparation) are presented in Table 2 and intended for construction of pseudo-sections only.

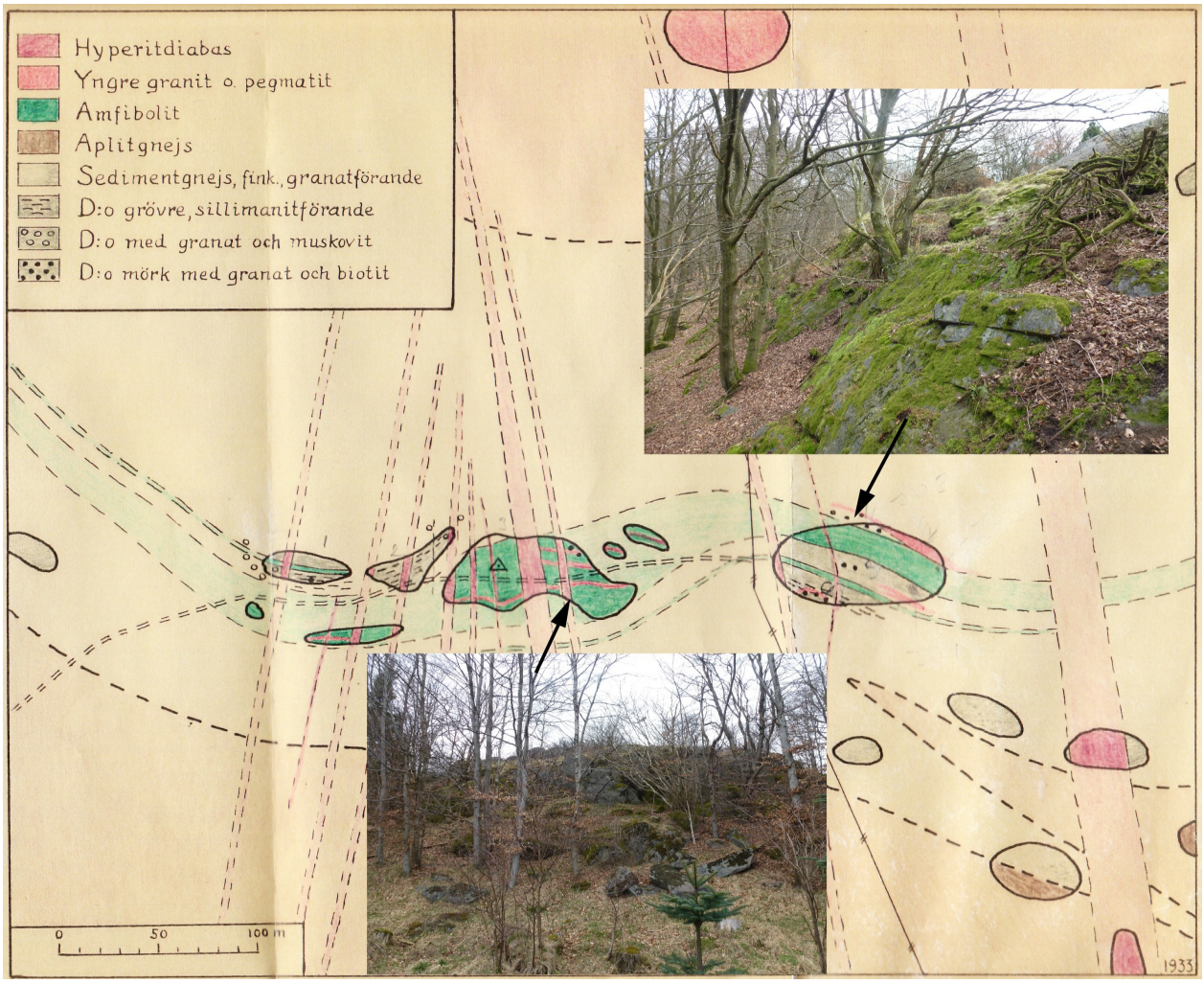

Fig. 3. Geological map of Romeleklint with sampled outcrops (from Hjelmqvist 1934). Inset photographs: Jan Ulmius.

Table 1. Sample data and rock description

Sample No.	Location	Coordinates SWEREF 99TM		Hand sample description	Thin section description
		N	E		
JU1	Romeleklint, eastern outcrop	6165130	402684	Fine-grained grey gneiss with Ms-filled fractures	Grt-bearing Sil-Bt gneiss
JU4	Romeleklint, eastern outcrop	6165135	402687	Deformed fine-grained grey gneiss	Grt-Sil-Bt gneiss
JU8B	Romeleklint, western outcrop	6165164	402460	Fine-grained grey gneiss with Grt	Grt-Sil-Bt gneiss
JU25Ab	Romeleklint, western slope	6165139	402404	Fine-medium-grained grey gneiss with Grt	Grt-Sil-Bt gneiss
JU25Aa	Romeleklint, western slope	6165139	402404	Fine-grained dark-grey gneiss	Grt-bearing Bt gneiss
JU25B	Romeleklint, western slope	6165139	402404	Fine-medium-grained grey gneiss with Grt	Grt-Sil-Bt gneiss
JU26A	Romeleklint, eastern outcrop	6165136	402687	Medium-grained gray gneiss with large Grt	Bt-Grt gneiss
JU26B	Romeleklint, eastern outcrop	6165136	402687	Fine-grained dark-grey gneiss with Grt	Bt-Grt gneiss
SB1AJU	Stenberget quarry, eastern wall	6158250	406477	Fine-medium grey gneiss with Grt	Grt-Sil-Bt gneiss
JU12	Nygård	6160626	407295	Fine-medium-grained spotted grey gneiss with Grt	Crd-Grt-bearing Ms-Bt-Ilm-Sil granofels
JU13	Nygård	6160608	407286	Fine-medium-grained spotted grey gneiss with Grt	Crd-Grt-bearing Ms-Bt-Ilm-Sil granofels
JU14	Nygård	6160577	407265	Fine-medium-grained spotted grey gneiss	Crd-Grt-bearing Ms-Bt-Ilm-Sil granofels
JU28	Nygård	6160577	407265	Fine-medium-grained spotted grey gneiss with Grt	Crd-Grt-bearing Ms-Bt-Ilm-Sil granofels
SB4	Stenberget quarry, eastern wall	6158250	406477	Fine-grained greys gneiss with Grt	Grt-bearing Sil-Ms-Bt gneiss
SB6	Stenberget quarry, eastern wall	6158250	406477	Fine-grained greys gneiss with Grt	Grt-bearing Sil-Ms-Bt gneiss
SB7	Stenberget quarry, eastern wall	6158250	406477	Fine-grained greys gneiss with Grt	Ms-Bt-Grt gneiss
SB8	Stenberget quarry, eastern wall	6158250	406477	Fine-grained greys gneiss with Grt	Grt-bearing Bt-Ms-Sil gneiss
JU9B	Romeleklint , western outcrop	6165113	402512	Fine-grained dark grey-green gneiss	Grt-bearing amphibolites

However, even in absence of trace element analyses the main elements can tell something about protolith and tectonic setting (see Giere et al. 2011 for recent applications). A chemical classification according to Herron (1988) shows that the protoliths were greywackes to shales (Fig. 4). The origin can be tested by a method developed by Roser and Korsch (1988), which applies a discriminant function using seven major element components to distinguish four sources for the sedimentary material (Fig. 5). According to this method the data plot mostly in the field of felsic igneous provenance (rhyodacite-rhyolite-granite). The data point with the lowest F2 value (sample JU9B) is an amphibolite which should be disregarded in this type of diagram as it is originally probably an intrusive rock. Sample JU26B (from the eastern outcrop of Romeleklint) is a narrow band in paragneiss with a mafic appearance (Fig. 6) although it is a Bt-Grt gneiss. Sample SB1AJU (from Stenberget) is also located in the mafic region in Fig. 5, but it has not a mafic appearance (Fig. 7). It deviates from other samples in its high alumina content. Sample JU26A is from an outcrop on Romeleklint with large garnet grains but without gneissic appearance (Fig. 8) and most likely represents a melt. Finally, sample JU25Aa, which is from a dark fine-grained band in the rock (Fig. 9), probably represents what Hjelmqvist (1934) referred to as leptite gneiss, a quartzofeldspathic metamorphic rock of volcanic origin. A K_2O/Na_2O vs SiO_2 discrimination diagram according to Roser and Korsch (1986) suggests that the pelites were deposited in an active continental margin setting (Fig. 10).

4.3 Petrography and mineral chemistry

4.3.1 Cordierite-bearing rocks

Cordierite bearing rocks have been found at two local-

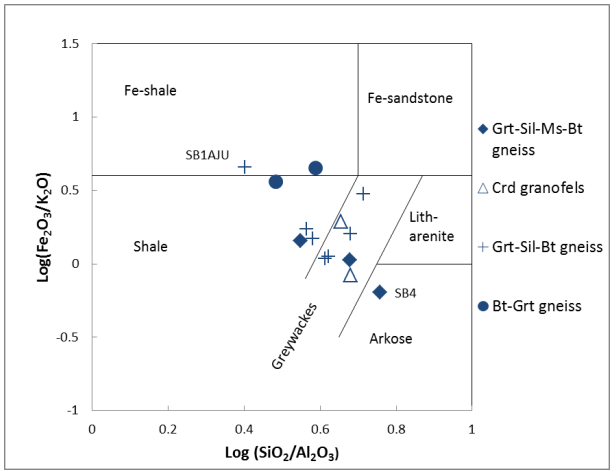

Fig. 4. Chemical classification of the metapelites from Romeleåsen using Fe_2O_3/K_2O versus SiO_2/Al_2O_3 according to Herron (1988).

Table 2. Bulk rock ICP analyses of samples from Romeleåsen.

	Grt-Sil-Bt gneisses								Grt-Bt gneiss	Crd-Grt bearing Ms-Bt-Ilm-Sil granofels					Amphibolite
	JU1	JU4	JU8B	JU25Ab	JU25B	JU25Aa	JU26A	SB1AJU	JU26B	JU12	JU28	SB4	SB7	SB6	JU9B
Major and minor oxides (wt%)															
SiO_2	67.69	65.85	68.02	66.56	72.47	73.69	59.23	58.64	58.55	69.92	70.93	75.07	70.88	64.69	46.25
TiO_2	0.51	0.58	0.53	0.66	0.46	0.48	0.68	0.93	1.55	0.54	0.47	0.39	0.30	0.76	1.68
Al_2O_3	16.50	17.93	16.25	17.51	15.14	14.25	19.50	23.21	15.15	15.47	14.80	13.12	14.90	18.30	15.96
Cr_2O_3	0.003	0.003	0.003	0.004	<0.002	0.003	0.003	0.004	0.004	<0.002	<0.002	0.002	<0.002	0.004	0.008
Fe_2O_3	4.30	5.03	4.34	5.29	3.19	2.32	5.78	7.69	10.45	4.35	3.54	2.00	3.80	4.93	14.28
MnO	0.08	0.13	0.12	0.14	0.07	0.03	0.24	0.23	0.12	0.11	0.07	0.04	0.20	0.14	0.19
MgO	1.34	1.80	1.23	1.46	0.88	0.49	1.01	1.79	2.88	0.83	0.71	0.60	1.55	1.36	8.24
CaO	1.74	1.34	1.94	1.28	2.15	3.58	3.62	0.59	5.02	2.08	1.56	1.60	1.26	1.31	8.09
Na_2O	2.35	2.30	2.44	1.61	2.33	3.44	4.98	0.81	1.42	2.34	2.08	2.97	2.78	3.19	2.10
K_2O	3.97	2.93	3.88	3.58	2.00	0.78	1.60	1.69	2.31	2.23	4.24	3.14	3.58	3.42	1.39
P_2O_5	0.08	0.04	0.07	0.07	0.05	0.04	0.10	0.03	0.43	0.05	0.06	0.07	0.02	0.04	0.38
LOI	1.1	1.8	0.8	1.5	1.0	0.7	3.0	4.2	1.8	1.8	1.3	0.7	0.5	1.6	1.1
Sum	99.66	99.73	99.62	99.66	99.74	99.80	99.74	99.81	99.68	99.72	99.76	99.70	99.77	99.74	99.67
Trace elements (ppm)															
Ba	1203	1255	1284	1144	670	208	583	304	583	761	1193	840	385	627	363
Ni	<20	<20	<20	<20	<20	<20	<20	<20	28	<20	<20	<20	<20	<20	163
Sr	287	182	297	210	255	327	288	54	274	185	277	288	152	194	279
Zr	262	185	308	318	296	428	82	523	241	240	263	355	152	335	148
Y	41	28	40	39	32	20	224	21	36	30	18	27	66	36	30
Nb	17	13	18	18	17	18	13	29	16	17	16	17	22	38	12
Sc	13	7	17	13	10	9	76	14	22	7	4	4	9	8	20

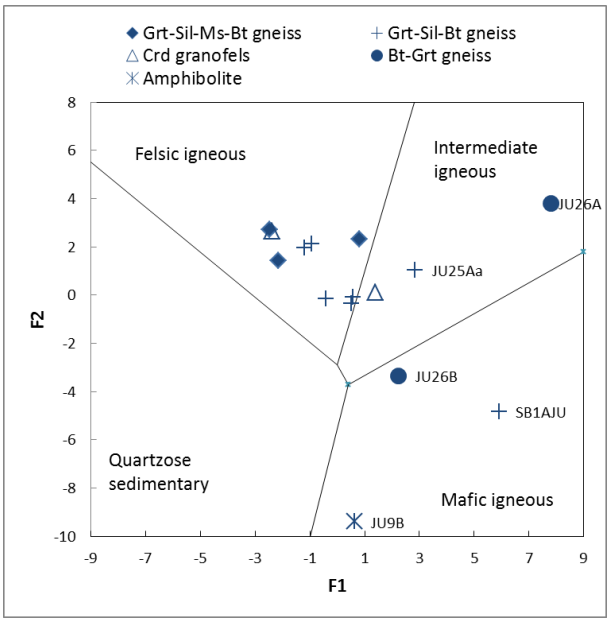

Fig. 5. Provenance discrimination diagram for gneisses from Romeleåsen using the discriminant functions $F1 = 0.607*Al_2O_3 - 1.773*TiO_2 + 0.76*Fe_2O_3^T - 1.5*MgO + 0.616*CaO + 0.509*Na_2O - 1.224*K_2O - 9.09$ and $F2 = 0.07*Al_2O_3 + 0.445*TiO_2 - 0.25*Fe_2O_3^T - 1.1.42*MgO + 0.438*CaO + 1.475*Na_2O + 1.426*K_2O - 6.861$ according to Roser and Korsch (1988). Numbers refer to samples discussed in the text.

Fig. 6. Garnet-biotite gneiss from Romeleklint (JU26B).

ities, Nygård and Stenberget. Representative microprobe data from Nygård are presented in Table 3.

4.3.1.1 Nygård

The Crd-Grt bearing Ms-Bt-Ilm-Sil granofels from

Fig. 7. Grey gneiss from Stenberget (SB1AJU).

Fig. 9. Fine to medium-grained grey gneiss from Romeleklint with a darker fine-grained band (JU25A).

Fig. 8. Outcrop with garnet porphyroblasts at Romeleklint (JU26A). Silva compass for scale.

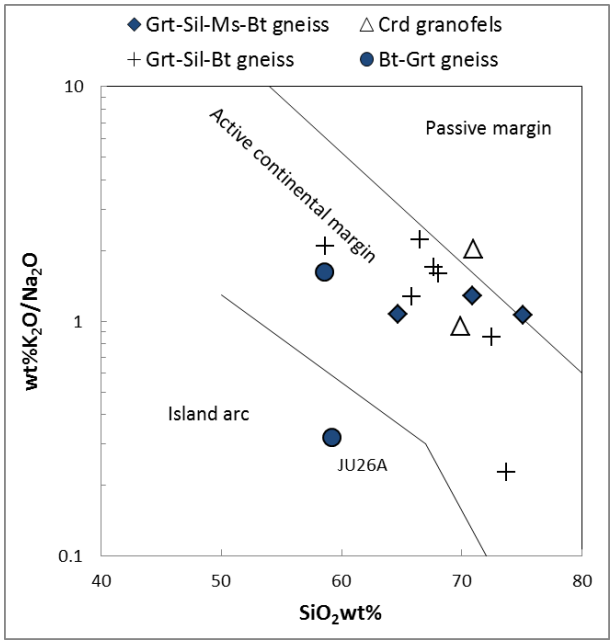

Fig. 10. Tectonic setting discrimination diagram using K_2O/Na_2O vs SiO_2 (Roser & Korsch 1986).

Nygård (samples JU12, JU13, JU14 and JU28) is a fine to medium grained yellowish-grey rock with bluish-grey specks (Fig. 11). In thin section the specks are spongy yellowish aggregates (Fig. 11). They consist of biotite, sillimanite and fine-grained muscovite with inclusions of quartz and sometimes Fe-Ti oxides (Fig. 12). Remnants of cordierite in the aggregates was identified using EDX spot analysis (Fig. 13), thus confirming that the bluish grey specks are pseudomorphs after cordierite as suggested by Hjelmqvist (1934). The presence of faint leucosomes suggest that the cordierite-garnet granofelses have been subjected to partial melting (Fig. 14).

Quartz and feldspars: The matrix of the cordierite-garnet granofelses is granoblastic with weakly undulose quartz, crypto- to microperthitic K-feldspar (Or_{80-90}), and plagioclase (An_{26-35}).

Biotite can be found in the matrix as up to 1 mm long flakes, often in aggregates with sillimanite, hematite and spinel. In the pseudomorphs after cordierite, biotite often forms a corona around Fe-oxides. Symplectites of biotite and plagioclase are also observed. Fe/(Fe+Mg) ratios are 0.5-0.6 in the matrix, 0.5 in the pseudomorphs and 0.40-0.45 close to garnet and in inclusions in garnet.

Cordierite is only found as relicts in pseudomorphs and show polysynthetic twinning. Fe/(Fe+Mg) ratios are 0.40-0.44.

Prismatic *sillimanite* can be found in aggregates with biotite; however in the pseudomorphs after cordierite sillimanite is fibrolitic.

Garnet occurs sparsely. One subhedral garnet about 1 mm in diameter can be observed in sample JU12 associated with a cordierite pseudomorph (Fig. 15). Inclusions in the garnet are biotite, hematite and spinel, and fine-grained intergrowths of rutile + corundum and ilmenite + rutile + quartz. The composition is Alm_{69-74}, Prp_{15-18}, Grs_{2-4} and Sps_{8-11} and the compositional profile is flat without zonation (Fig. 16). The garnet grain in sample JU13B has a long tail rich in

Table 3. Representative EDS microprobe data for minerals in cordierite-garnet bearing granofelses from Nygård.

Mineral	**Grt**	**Bt**	**Bt**	**Bt**	**Pl**	**Crd**	**Crd**	**Spl**	**Spl**	**Spl**	**Spl**	**Spl**	**Ilm**	**Ilm**	**Rt**	**Rt**	**Hem**	**Hem**
Sample	JU12	JU12	JU12	JU12	JU12	JU14	JU28A	JU12	JU12	JU13B	JU14	JU28A	JU12	JU12	JU12	JU12	JU12	Ju12
Analytical	9035	9035	9035	9035	9035	8020	1060	9035	9535	5090	8020	1090 2	9535	9535	9535	9535	9535	9535
site	(n=14)	Grt incl (n=9)	Grt close (n=5)	Matrix (n=5)	Matrix (n=9)	Matrix (n=2)	Matrix (n=3)	Grt incl (n=3)	Matrix (n=2)	Matrix (n=9)	(n=3)	(n=1)	Grt incl (n=2)	Matrix (n=2)	Grt incl (n=4)	Matrix (n=2)	Grt incl (n=3)	Matrix (n=3)
SiO_2	36.14	35.49	34.93	34.58	58.34	46.64	46.13											0.12
TiO_2		3.33	3.24	3.47	0.05								51.61	51.94	95.00	97.08	0.14	0.15
Al_2O_3	21.13	18.75	17.61	17.73	25.31	32.40	32.19	58.19	58.17	55.51	55.68	56.66	0.18	0.17	0.55		0.56	0.50
Cr_2O_3								0.36			0.40							
FeO tot	32.25	16.82	17.77	20.99		8.85	9.33	33.04	35.51	32.10	31.51	28.49	32.73	34.20	2.88	3.61	94.06[1]	97.59[1]
MnO	4.14			0.09		0.57	0.19		1.19		1.12	0.87	13.51	13.27				
MgO	3.52	12.24	10.89	9.22		7.43	7.20	4.28	2.79	3.66	2.50	2.27	0.215					
CaO	0.95				6.72													
Na_2O					7.99													
K_2O		9.52	9.16	9.71	0.08													
V_2O_5		0.06													0.98		3.73	0.22
ZnO								2.88	4.11	5.36	7.76	11.66						
Total	98.12	96.22	93.59	95.78	98.58	95.89	95.04	98.76	101.8	96.64	98.69	99.95	98.24	99.58	99.40	100.69	98.49	98.55
O for calc[1]	12	11	11	11	8	18	18	4	4	4	4	4	3	3	2	2	3	3
Si	2.96	2.65	2.69	2.65	2.63	4.94	4.86											
Ti		0.19	0.19	0.20	0.00								0.99	0.99	0.97	0.98		
Al	2.04	1.65	1.60	1.61	1.35	4.05	3.99	1.96	1.94	1.93	1.92	1.94	0.01	0.01	0.01		0.02	0.01
Cr								0.01			0.01							
Fe^{2+}	2.16	1.05	1.15	1.35		0.72	0.82	0.79	0.84	0.72	0.77	0.63	0.69	0.72	0.03	0.04		
Fe^{3+}	0.05	0.00	0.00	0.00		0.07	0.22	0.01	0.01	0.07	0.02	0.06	0.01	0.01			1.87	1.97
Mn	0.29			0.01		0.05	0.02		0.03		0.03	0.02	0.29	0.28				
Mg	0.43	1.36	1.25	1.06		1.17	1.13	0.18	0.12	0.16	0.11	0.10	0.01					
Ca	0.08				0.33													
Na					0.70													
K		0.91	0.90	0.95	0.00													
V		0.00													0.01		0.07	
Zn								0.06	0.09	0.12	0.17	0.25						
Total cati-ons	8.00	7.80	7.77	7.82	5.03	11.00	11.04	3.01	3.02	3.00	3.03	3.00	2.00	2.01	1.02	1.02	1.96	2.00
Fe/(Fe+Mg)	0.84	0.44	0.48	0.56		0.40	0.42	0.81	0.88	0.82	0.88	0.86						
Alm	0.73																	
Prp	0.14																	
Grs	0.03																	
Sps	0.10																	
An					0.32													
Ab					0.68													
Spinel								0.18	0.11	0.16	0.10	0.10						
Hercynite								0.75	0.77	0.72	0.71	0.63						
Gahnite								0.07	0.08	0.12	0.16	0.25						
Galaxite									0.03		0.03	0.02						

[1]Cation compositions include a stoichiometric estimate of Fe3+ calculated with the AX software (Holland 2012).

sillimanite (Figure 17) suggesting that the garnet has been partly resorbed to produce fine-grained aggregates of sillimanite, spinel and iron-titanium oxides. The garnet composition is Alm_{70-75} Prp_{13-16} Grs_3 Sps_{8-10}.

Spinel can be found in different textures and assemblages. In sample JU12 spinel is found as a pure inclusion in garnet and also as an inclusion assemblage with biotite and hematite with fine-grained ilmenite, rutile, corundum and quartz (Fig. 15). In sample JU12 as well as in samples JU14 and JU28 spinel is associated with biotite, sillimanite, hematite, and ilmenite with fine-grained rutile and quartz (Fig. 18). In sample JU13B spinel can be found as an assemblage with garnet, sillimanite, hematite, and fine-grained rutile, sillimanite, and quartz. Spinel compositions vary, with 9-17 mol% Mg-spinel, 67-77 mol% hercynite (Fe-spinel), and 6-24 mol% gahnite (Zn-spinel). Small amounts of galaxite (Mn-spinel) was found in sample JU14.

Accessory minerals: Zircon is abundant and forms rounded grains 20-100 µm. Ilmentite, rutile and Fe-oxides are abundant and often associated with biotite and spinel. Ilmenite contains about 30 mol% pyrophanite ($MnTiO_3$). The Fe-oxides is best calculated as hematite (98.5% Fe_2O_3). Pyrite has been found in one thin section.

4.3.1.2 Stenberget

Rocks with spongy aggregates similar to those at Nygård can be found in the quarry at Stenberget (SB4, SB6, SB7 and SB8). The aggregates are most probably pseudomorphs after cordierite. However, they are greenish in thin section instead of yellowish (Fig. 19). The Stenberget cordierite rocks are more gneissose than the rocks at Nygård.

Quartz and feldspars in the matrix are similar to

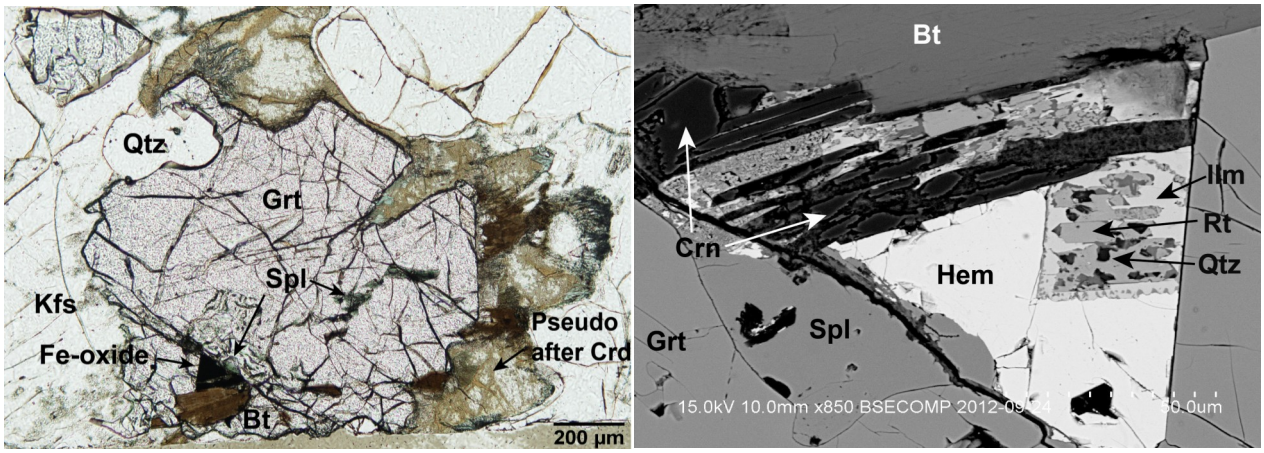

Fig. 15. Photomicrograph showing garnet with spinel inclusion in cordierite-sillmanite gneiss from Nygård sample JU12. To the right back-scattered electron (BSE) image of area with inclusions of spinel, biotite, and hematite with corundum, ilmenite, rutile and quartz.

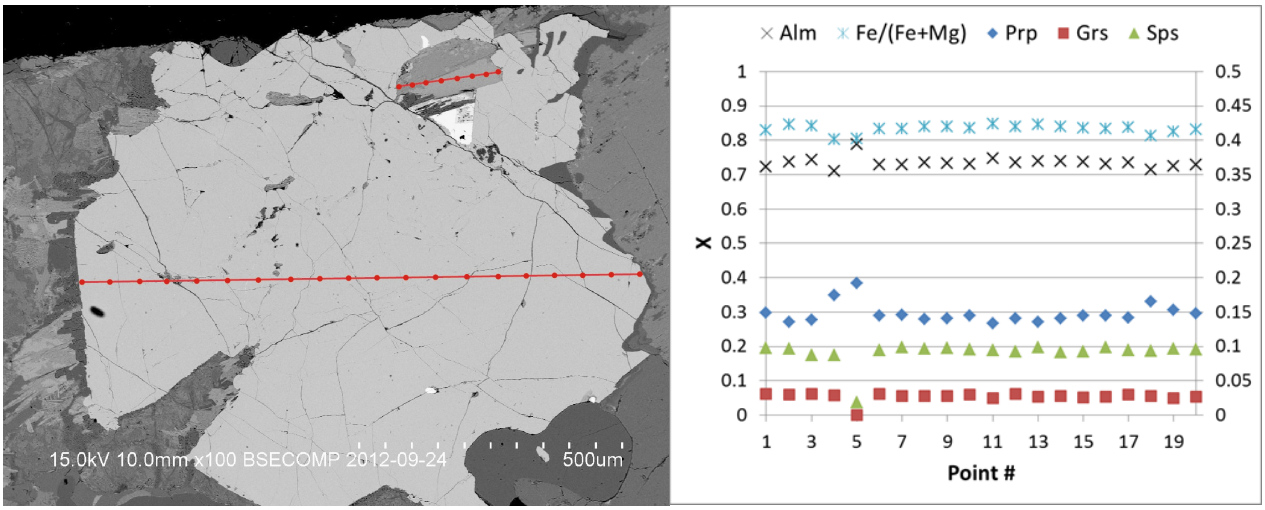

Fig. 16. BSE-image of garnet in cordierite-sillmanite gneiss from Nygård sample JU12. Red labelled spots for the garnet and the biotite inclusion indicate analyses for thermobarometry. To the right the compositional profile of garnet in sample JU12 from rim at sillimanite (left) to rim at K-feldspar (right). Fe/Fe+Mg) ratios (left axis) and mole fractions of almadine (left), pyrop (right axis), grossular (right) and spessartine (right). Point 4 and 5 at Spl inclusion.

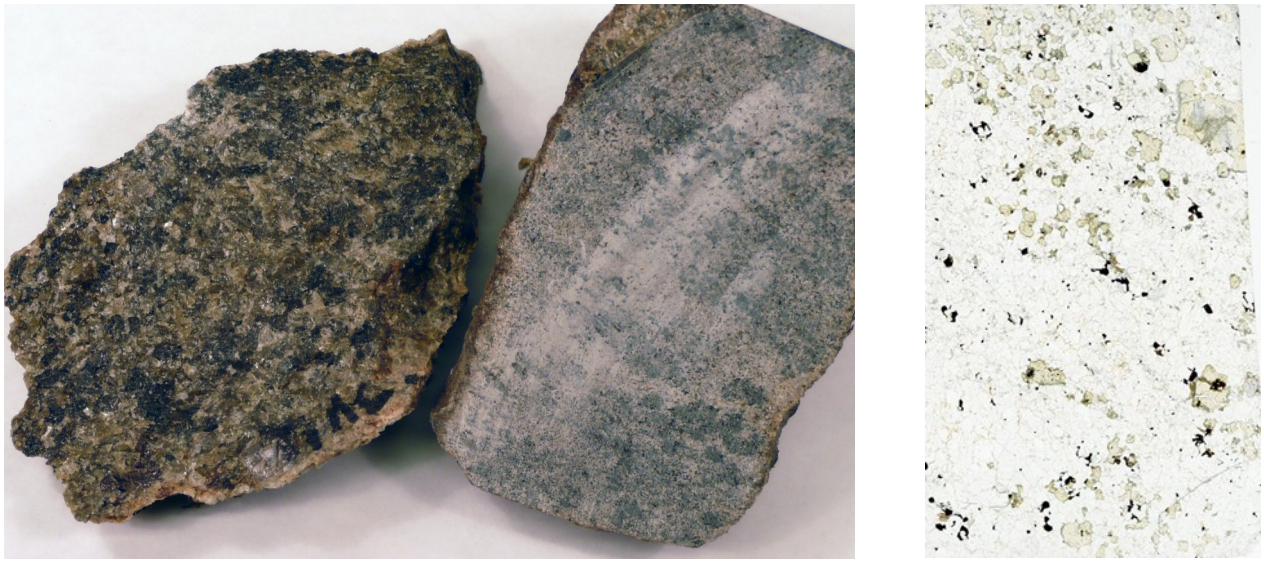

Fig. 11. Cordierite-sillimanite gneiss from Nygård (JU12). To the right a thin section of the rock. Width 21 mm.

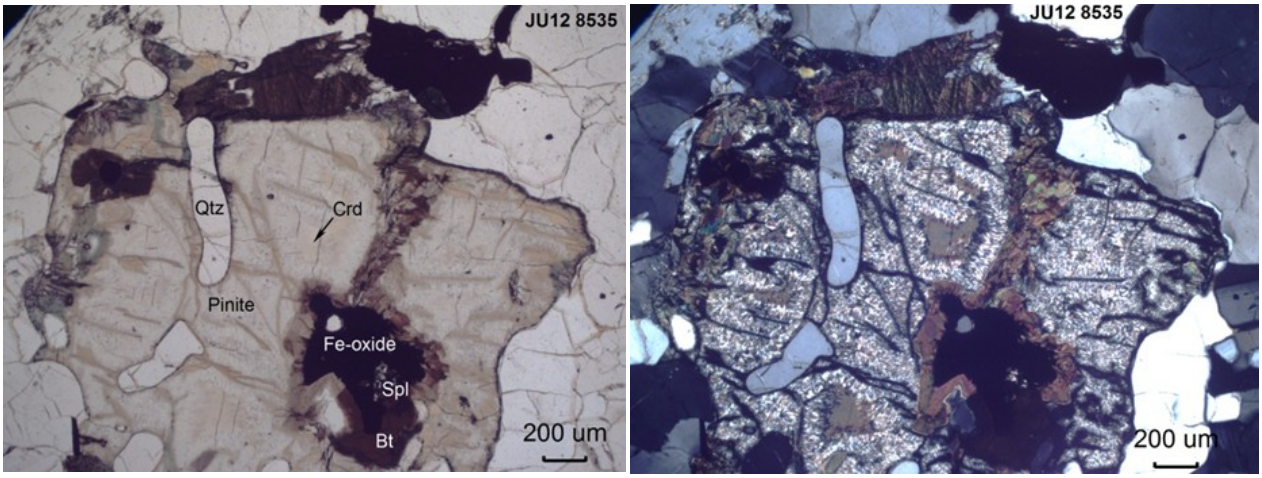

Fig. 12. Photomicrograph of yellowish aggregate (pseudomorph after cordierite) in sample JU12 (Fig. 11) in plane-polarised (left) and cross-polarised light (right).

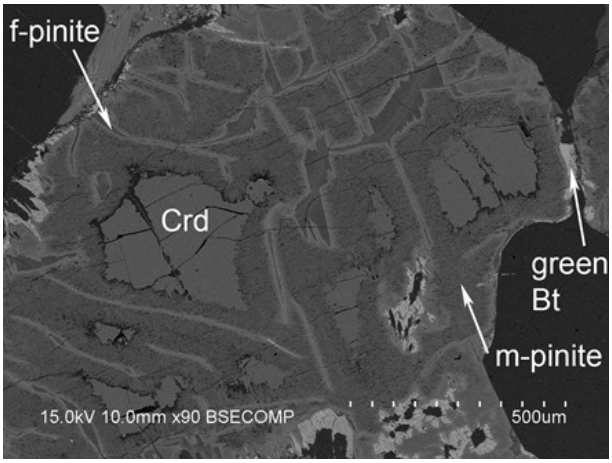

Fig. 13. Back-scattered electron image of a yellowish aggregate (pseudomorph after cordierite) in cordierite-sillimanite gneiss from Nygård (sample JU28). For explanation of f- and m-pinite, see text.

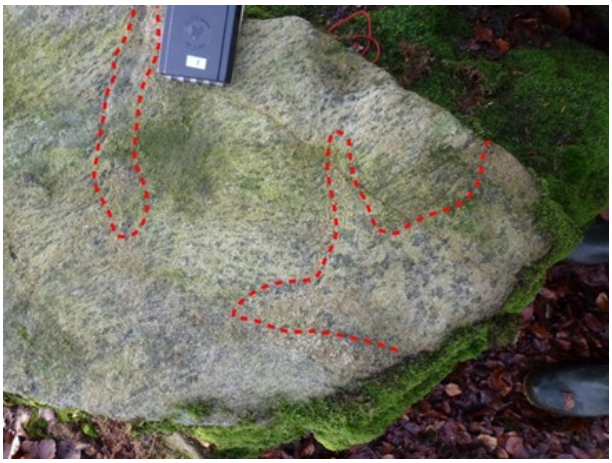

Fig. 14. Cordierite-sillimanite rock at Nygård showing faint patches of leucosome outlined with red dashes. Silva Compass for scale.

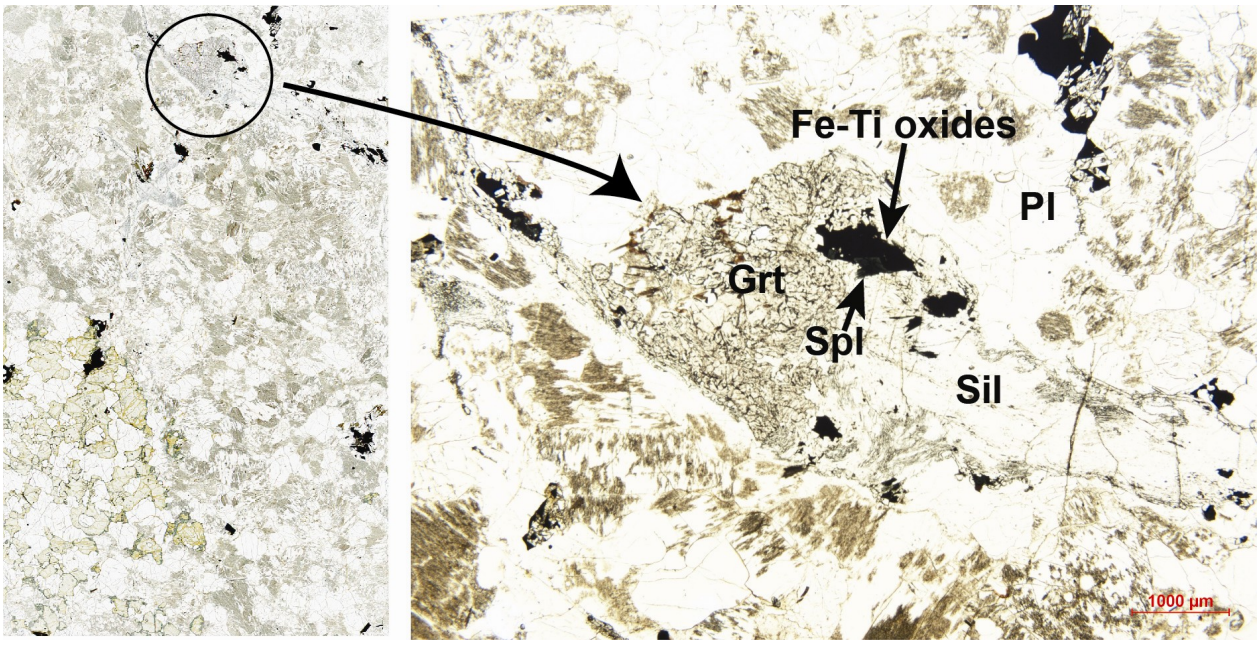

Fig. 17. Thin section of cordierite-sillimanite gneiss from Nygård (sample JU13B) with resorbed garnet at the top; width 21 mm. The photomicrograph to the right shows the resorbed and strongly anhedral garnet, with secondary sillimanite, spinel and opaques surrounded by plagioclase.

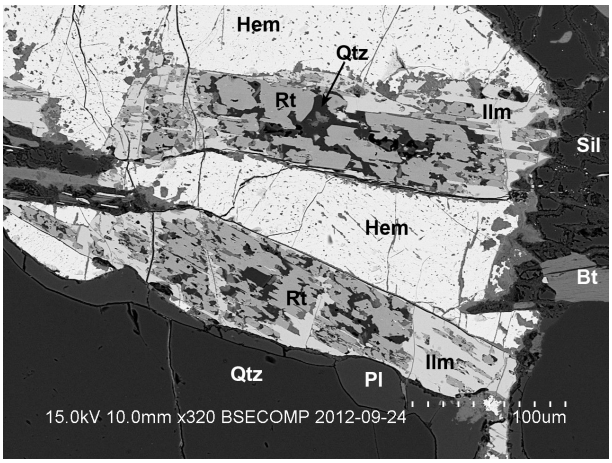

Fig. 18. BSE-image of an assemblage of spinel-hematite-ilmenite with rutile and quartz in cordierite-sillimanite gneiss sample JU12 from Nygård. The spinel is just above the upper edge of the image.

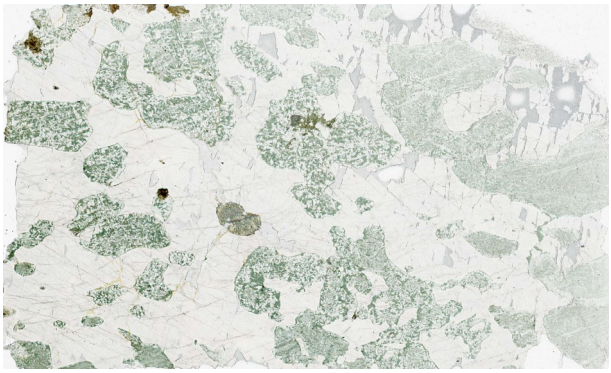

Fig. 19. Thin section of cordierite-sillimanite gneiss from Stenberget (sample SB6). Height 20 mm.

what is found in the rocks from Nygård.

Biotite appears as brown flakes of different sizes in the matrix and as inclusions in garnet; Fe/(Fe+Mg) is 0.5-0.6. A green variety of biotite can be found in the spongy aggregates and has also been observed as a corona around a garnet. The Fe/(Fe+Mg) ratio is 0.4-0.5 and titanium is absent or very low.

Muscovite occurs in small flakes together with green biotite in the spongy aggregates and has the approximate composition muscovite 90 mol%, celadonite 5 mol% and paragonite 5 mol%.

Sillimanite is sparser than in the Nygård samples but can be found both as prismatic grains and as finer needles.

Garnet can be found in different sizes (mm-cm). The smaller garnet grains are sub- to euhedral and contain inclusions of biotite and quartz. The larger garnet grains in the matrix are often skeletal with quartz inclusions. In one thin section (SB8A) garnet, biotite and sillimanite define a foliation and the garnets have inclusions of biotite, muscovite, quartz, Fe-Ti-oxides and spinel. The compositional profile is almost flat for all garnets, with Alm 75-80 mol%, Prp 10-15 mol%, Grs 2-3 mol% and Sps 5-10 mol%. However, pyrope commonly show a slight decrease close to the rim while almandine increases. Spessartine content increases at the rim. One garnet grain (sample SB6B) is high in spessartine with the composition $Alm_{58-61}Prp_{9-10}Grs_{2-4}Sps_{27-30}$.

Spinel can be found in similar textural relations as observed for Nygård, i.e. in inclusions in garnet together with biotite, muscovite, Fe-oxides, ilmentite, rutile and corundum. The composition is 7-9 mol% Mg-spinel, 49-51 mol% hercynite, and 39-43 mol%

gahnite i.e. high in Zn.

Staurolite has been found as an inclusion in garnet (SB6) with the composition 71 mol% Fe-endmember, 20 mol% Mg-endmember, 5 mol% Mn-endmember, and 4 mol% Zn-endmember..

Accessory minerals and their associations are the same as observed for Nygård. Ilmenite contains about 5 mol% pyrophanite.

4.3.2 Garnet-bearing sillimanite-biotite gneisses

Most paragneisses outcropping at Romeleklint have a pronounced foliation (Fig. 20 to Fig 23). However, there are also rocks without any evident foliation or lineation (Fig. 24). Foliations and lineations are commonly defined by biotite and sillimanite anastomosing around porphyroclasts of partly resorbed garnet. Representative microprobe data is presented in Table 4.

Sillimanite occurs in fibrolite bundles and as prismatic grains 50-200 µm in length.

Biotite forms irregular flakes 10 µm – 1.5 mm or fine recrystallized grains. Fe/(Fe+Mg) ratios for biotite vary between 0.5 and 0.6.

Quartz forms irregular elongate undulous grains from a few µm to mm and also fine recrystallized grains.

Plagioclase is clear with some seritization and with An_{25-35}.

K-feldspar is kryptoperthitic with Or_{80-90}.

Muscovite occurs mainly as fine grains in aggregates, occasionally as larger flakes up to 0.5 mm. The approximate composition is muscovite 90 mol%, celadonite 5 mol% and paragonite 5 mol%.

Garnet grains in the deformed paragneisses vary in size from 0.5 mm to a few millimeters. The large ones are often fractured and contain inclusions of quartz, biotite, sillimanite needles and opaques. Small garnet grains are euhedral to subhedral and also have inclusions of quartz, biotite, sillimanite and opaques. The Fe/(Fe+Mg) ratio is 0.82-0.91 and the composition is $Alm_{68-81}Prp_{7-19}Grs_{2-8}Sps_{2-20}$. Compositional profiles are generally flat but in some cases along rims and cracks there are increasing contents of Alm, Grs and Sps and a decreasing content of Prp (Fig. 25).

Spinel is found locally in association with sillimanite and biotite or muscovite in the matrix and as inclusions in garnet. Spinel is associated with very fine-grained *staurolite and corundum* (Fig. 26). Mg-spinel varies from 5 to 11 mol%, hercynite from 29 to 35 mol% while the gahnite content is very high; 54-64 mol%. In staurolite the Mg-endmember is 11-17 mol%, the Fe-endmember is 66-67 mol% and the Zn-endmember is 15-22 mol%.

Accessory minerals include ilmenite (pyrophanite 3 -20 mol%), rutile, Fe-oxides, zircon and monazite.

Specimens JU8A and JU25A contain a fine-grained dark band (Fig. 23), which probably is a leptite according to Hjelmqvist. The matrix is granoblastic with fine-grained quartz and clear plagioclase (An_{36-39}). Biotite flakes, 5-50 µm, with Fe/(Fe+Mg) ratio 0.56-0.64 are evenly distributed. Garnet grains are subhedral, 0.1-0.5 mm, with an Fe/(Fe+Mg) ratio of 0.84-0.89. The composition is $Alm_{76-78}Prp_{8-14}Grs_{3-8}Sps_{5-10}$ with a flat compositional profile.

The medium-grained and non-foliated biotite-garnet gneiss (sample JU26A, Fig. 24) contains large irregular grains of quartz and plagioclase in the matrix. The plagioclase has suffered substantial seritization and/or sassuritization. Light-brown to brown biotite vary in grain size. Garnet grains are rounded, 1-10 mm, and host inclusions of biotite, quartz and muscovite. Biotite is absent in some garnet-bearing quartz-feldspar domains; these may represent melt (leucosome).

The dark specimen JU26B, taken close to JU26A, has a granoblastic matrix of fine-grained undulous quartz and clear plagioclase. Small flakes of biotite are abundant between quartz and plagioclase, and seem to have gathered in zones. Garnet is abundant. There are both large fractured garnet grains with inclusions of quartz and biotite, and small rounded dusty grains. Opaque minerals are also abundant.

Fig. 20. Outcrop on the western part of Romeleklint showing a foliation with strike 280° and dip 80° N.

Table 4. Representative EDS microprobe data for minerals in the biotite-sillimanite-garnet gneiss.

Mineral	**Grt**	**Grt**	**Grt**	**Grt**	**Bt**	**Bt**	**Bt**	**Pl**	**Pl**	**Ms**	**Spl**	**Spl**	**St**	**St**
Sample	JU25A2	JU25A2	JU25A2	JU25A1	JU25A2	JU25A2	JU25A1	JU25A2	JU25A1	JU25A1	JU25A1	JU25A2	JU25A1	JU25A2
Analytical site	2535 Grt core (n=9)	2535 Grt rim Qtz (n=1)	2535 Grt rim Ms (n=1)	4090 Grt core (n=12)	2535 matrix (n=6)	2535 Grt incl (n=2)	4090 matrix (n=5)	2535 matrix (n=5)	4090 matrix (n=5)	4090 matrix Grt (n=5)	7525 (n=8)	2575 (n=2)	7525 (n=7)	2575 (n=3)
SiO_2	36.40	36.01	36.11	35.94	34.21	34.10	34.57	57.65	56.63	44.00			25.86	26.02
TiO_2					3.18	2.74	3.62			1.07			0.62	0.44
Cr_2O_3											0.82		0.66	
Al_2O_3	20.96	20.98	20.90	21.02	17.96	18.15	18.33	25.03	25.90	32.14	56.20	55.51	54.68	53.60
FeO tot	34.26	33.59	33.76	34.31	18.50	15.82	22.04			2.53	16.01	14.63	11.22	10.93
MnO	2.95	3.07	3.16	4.11								0.72		
MgO	3.37	3.25	2.47	2.63	9.41	10.52	7.15			0.75	2.13	2.42	0.81	1.53
CaO	1.02	1.03	2.18	1.18				7.11	7.91					
Na_2O								7.69	7.14	0.31				
K_2O					9.72	9.49	10.12		0.26	11.21				
ZnO											26.22	25.31	3.25	3.13
Total	98.95	97.93	98.58	99.19	92.98	90.83	95.83	97.49	97.69	91.76	101.28	98.23	96.89	95.65
O for calc[1]	12	12	12	12	11	11	11	8	8	11	4	4	23.5	23.5
Si	2.96	2.94	2.94	2.93	2.67	2.69	2.67	2.64	2.60	3.08			3.73	3.79
Ti					0.19	0.16	0.21		0.00	0.06			0.07	0.05
Al	2.01	2.02	2.01	2.02	1.65	1.69	1.67	1.35	1.40	2.65	1.92	1.95	9.30	9.21
Cr											0.02	0.02	0.07	
Fe^{2+}	2.26	2.29	2.30	2.23	1.21	1.04	1.42			0.15	0.39	0.36	1.35	1.33
Fe^{3+}	0.07	0.07	0.07	0.12	0.00	0.00	0.00				0.04	0.02		
Mn	0.20	0.21	0.22	0.28										
Mg	0.41	0.40	0.30	0.32	1.10	1.24	0.82			0.08	0.09	0.11	0.15	0.33
Ca	0.09	0.09	0.19	0.10				0.35	0.39					
Na								0.68	0.63	0.04				
K					0.97	0.95	1.00		0.01	1.00				
Zn							0.00				0.56	0.57	0.35	0.34
Total cations	8.00	8.02	8.02	8.00	7.79	7.78	7.79	5.02	5.03	7.06	3.01	3.03	15.01	15.05
Fe/Fe+Mg)	0.85	0.85	0.88	0.87	0.52	0.46	0.63			0.65	0.81	0.76		
Alm	0.76	0.77	0.76	0.76										
Prp	0.14	0.13	0.10	0.11										
Grs	0.03	0.03	0.06	0.04										
Sps	0.07	0.07	0.07	0.10										
An								0.34	0.38					
Ab								0.66	0.62					
Or									0.01					
XMg											0.09	0.10	0.07	0.17
XFe											0.37	0.35	0.68	0.67
XZn											0.54	0.55	0.18	0.17

[1]Cation compositions include a stoichiometric estimate of Fe3+ calculated with the AX software (Holland 2012).

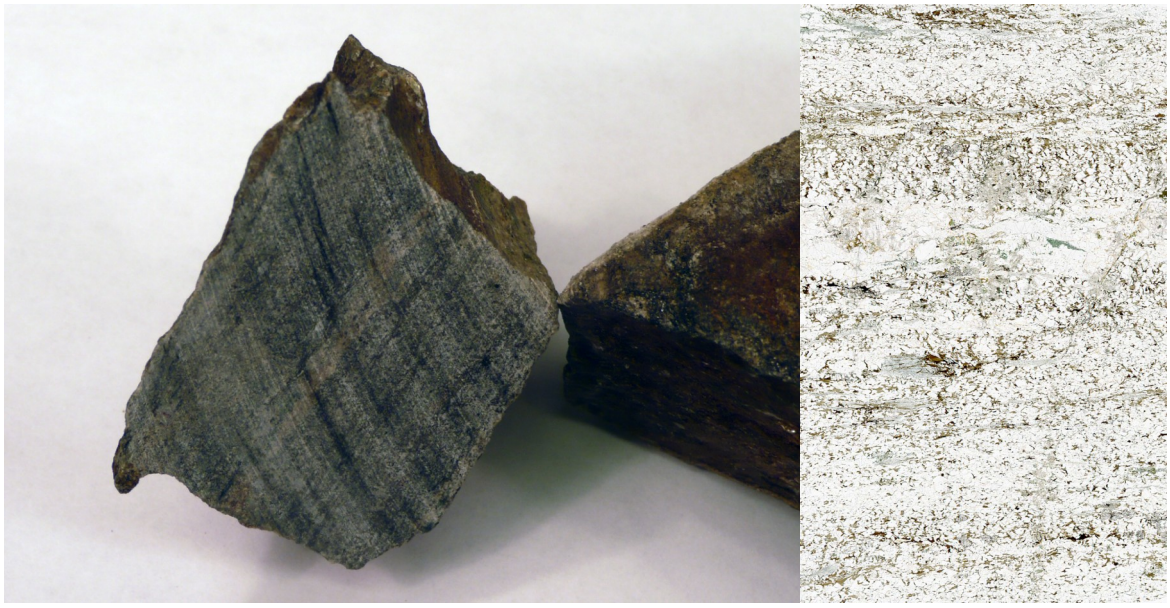

Fig. 21. A fine-grained grey gneiss from Romeleklint (JU1) with thin section (width 21 mm).

Fig. 22. A deformed fine-grained grey gneiss from Romeleklint (JU4) with thin section (width 20 mm)

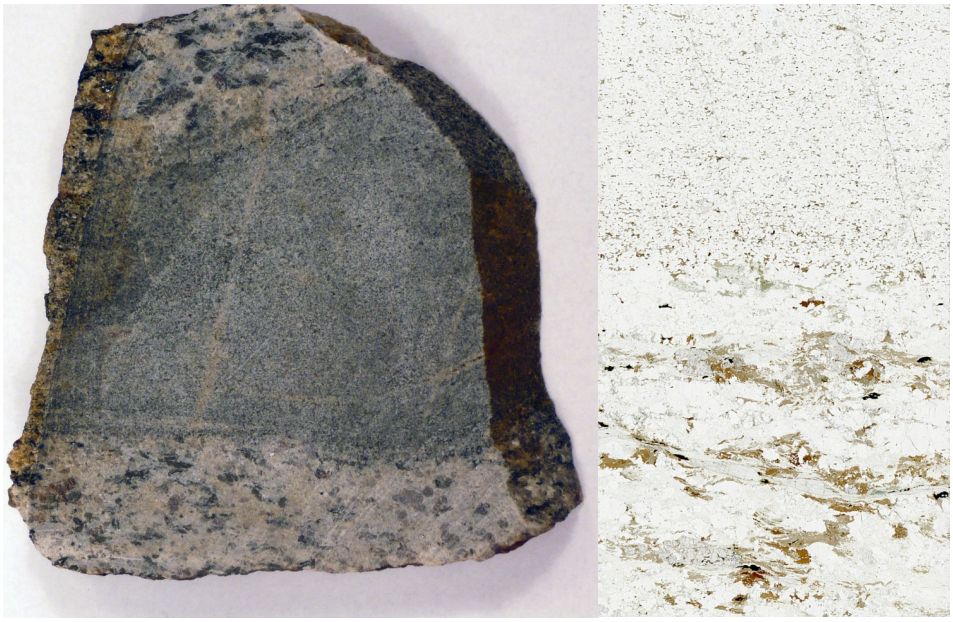

Fig. 23. Fine to medium-grained grey gneiss from Romeleklint with a darker fine-grained band (JU25A). Thin section (JU25A1) of the same sample. The lower part corresponds to the medium-grained part of JU25A and is named JU25Ab. The upper part corresponds to the fine-grained band of JU25A and is named JU25Aa. Width 21 mm.

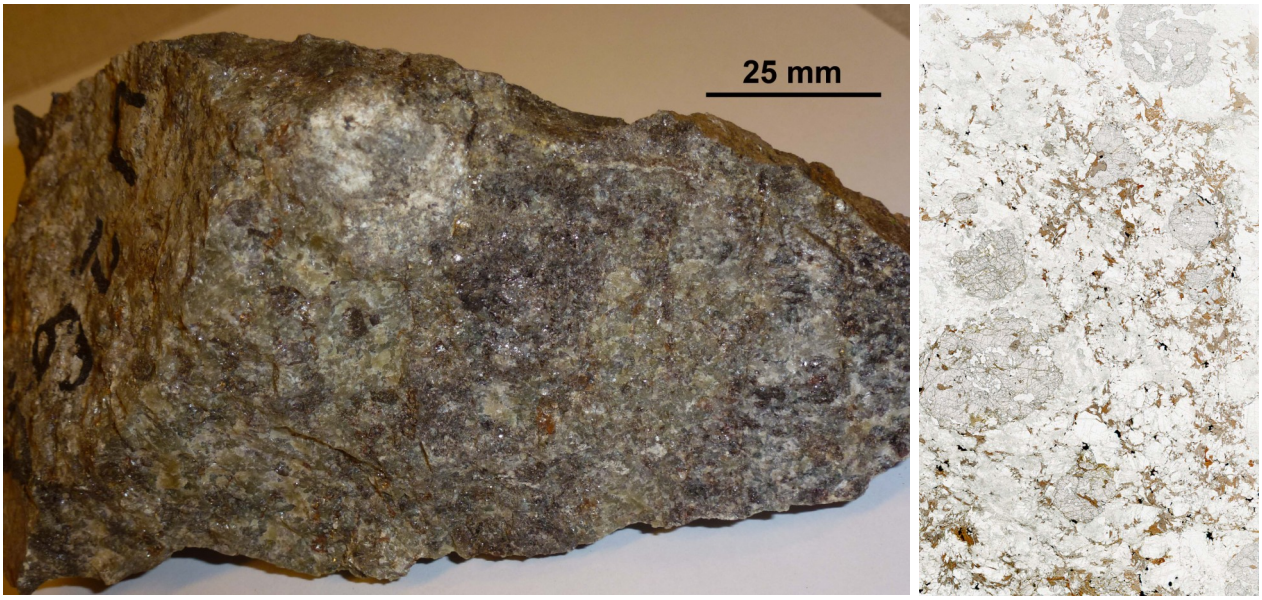

Fig. 24. Medium-grained grey gneiss from Romeleklint (JU26A) with thin section (width 21 mm).

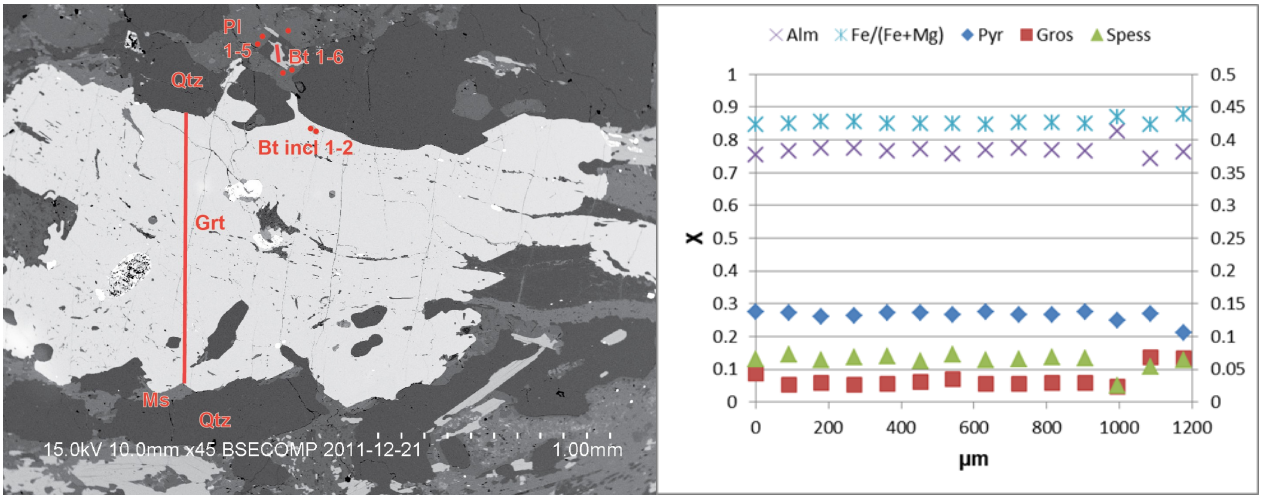

Fig. 25. BSE-image of garnet no. 2535 in thin section JU25A2 of fine- to medium-grained grey gneiss (JU25Ab). Red labelled spots and lines were used for thermobarometry. To the right a compositional profile from rim at quartz (top) to rim at muscovite (bottom). Fe/(Fe+Mg) ratios (left axis) and mole fractions of almadine (left), pyrope (right axis), grossular (right) and spessartine (right).

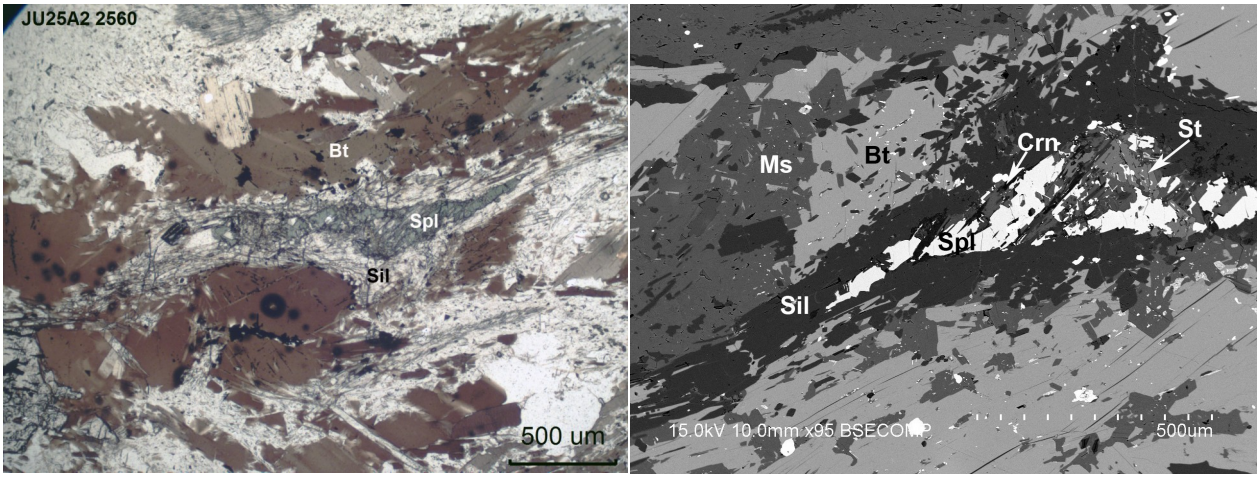

Fig. 26. Aggregates of spinel, sillimanite and biotite in medium-grained grey gneiss (JU25Ab, thin section JU25A2) from Romeleklint. To the right BSE-image (close-up) of the same domain.

4.3.3 Amphibolite

Hjelmqvist (1934) described cummingtonite- hypersthene- and anthophyllite amphibolite from Romeleklint. Sample JU9B is a dark fine-grained foliated rock (Fig. 27) and contains cummingtonite. The matrix is equigranular with elongated grains and a foliation defined by amphibole and biotite. Representative microprobe data is presented in Table 5.

Amphiboles are hornblende (magnesiohornblende to edenitic hornblende) and cummingtonite. Hornblende forms olive-green to brownish anhedral grains, sometimes twinned; Fe/(Fe+Mg) is 0.42-0.49. Cummingtonite forms colourless anhedral aggregates consisting of smaller flakes. The Fe/(Fe+Mg) ratio is 0.43 -0.45.

Biotite forms reddish brown to light brown flakes. The Fe/(Fe+Mg) ratio is 0.39-0.45.

Garnet grains, which are few in number, are about 0.5 mm, sub- to anhedral, and have inclusions of amphibole, plagioclase, biotite and ilmenite. The Fe/(Fe+Mg) ratio is 0.79-0.86 and the composition is $Alm_{65-72}Prp_{11-18}Grs_{10-17}Sps_{3-6}$. The cores are homogeneous in composition; one garnet grain has rims with higher Alm and Sps and lower Prp and Grs (Fig. 28).

Plagioclase is clear, sometimes with bent and complex twins. The composition varies between andesine (An_{30-50}) and labradorite (An_{50-70}).

Isolated relicts of *orthopyroxene* (enstatite-hypersthene) with Fe/(Fe+Mg) ratio 0.48-0.50 have also been observed.

Accessory minerals include ilmenite, apatite and dolomite. Dolomite is probably the result of secondary fluid deposition in veins; dolomite-bearing veins have also been described by Hjelmqvist (1934).

Fig. 27. Amphibolite from Romeklint (JU9B) with thin section to the right (width 20 mm).

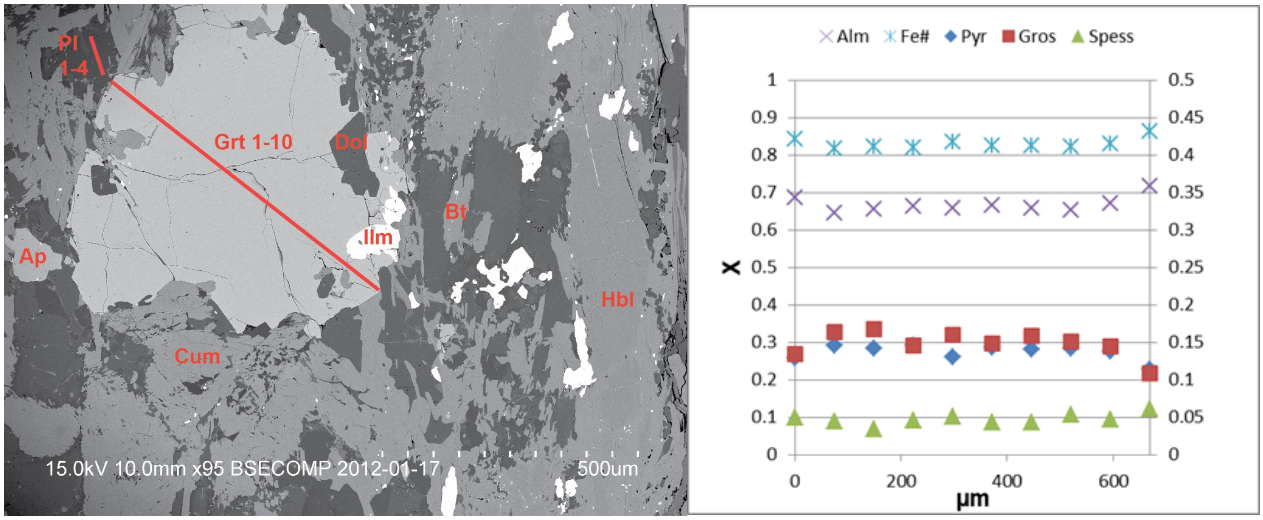

Fig. 28. BSE-image of garnet 8025 in amphibolite JU9B. Lines for thermobarometry labelled in red. To the right compositional profile from rim at plagioclase (left) to rim at biotite (right). Fe/(Fe+Mg) ratios (left axis) and mole fractions of almadine (left), pyrop (right axis), grossular (right) and spessartine (right).

Table 5. Representative EDS microprobe data for minerals in amphibolite.

Mineral	**Grt**	**Grt**	**Bt**	**Pl**	**Mg-Hbl**	**Cum**	**En**
Sample	JU9B	JU9B	JU9B	JU9B	JU9B	JU9B	JU9B
Analytical site	8025 Grt core (n=8)	8025 Grt rim (n=2)	8025 Matrix (n=6)	8025 Matrix (n=4)	8025 Matrix (n=4)	8025 Matrix (n=4)	1070 (n=4)
SiO_2	36.84	36.35	35.78	57.91	44.34	51.24	50.08
TiO_2			3.73		1.05		
Al_2O_3	20.93	20.87	15.69	25.37	10.27	1.11	0.81
FeO tot	29.83	31.48	17.30		15.31	24.02	30.00
MnO	2.02	2.43				0.60	0.73
MgO	3.57	3.05	12.52		11.55	17.01	17.09
CaO	5.47	4.28		6.85	10.97	0.63	0.40
Na_2O				8.10	1.36		
K_2O			9.49		0.45		
Total	98.66	98.45	94.52	98.23	95.31	94.33	99.12
O for calc[1]	12	12	11	8	23	23	6
Si	2.97	2.93	2.70	2.63	6.66	7.61	1.91
Ti			0.21		0.12		
Al	1.99	1.99	1.40	1.36	1.82	0.20	0.04
Fe^{2+}	1.93	2.13	1.09		1.54	2.98	0.96
Fe^{3+}	0.08	0.08	0.08		0.39	0.38	0.10
Mn	0.14	0.17				0.08	0.02
Mg	0.43	0.37	1.41		2.59	3.76	0.97
Ca	0.47	0.37		0.33	1.77	0.10	0.02
Na				0.71	0.40		
K			0.92		0.09		
Total	8.00	8.03	7.81	5.04	15.49	15.11	4.02
Fe#	0.82	0.85	0.44		0.37	0.44	0.50
Alm	0.65	0.70					
Prp	0.14	0.12					
Grs	0.16	0.12					
Sps	0.05	0.05					
An				0.32			
Ab				0.68			

[1]Cation compositions include a stoichiometric estimate of Fe^{3+} calculated with the AX software (Holland 2012).

4.4 Petrological interpretation

4.4.1 Bulk rock geochemistry

Using the methods of Herron (1988) and Roser & Kosch (1988), the bulk rock chemistry suggests that the protoliths for the main part of the paragneisses were greywackes and shales, derived from rhyodacitic to rhyolitic/granitic sources, and deposited in an active continental margin setting. One sample (JU25Aa) of a paragneiss with intermediate (andesitic to dacitic) composition has probably a volcanic origin.

4.4.2 Textures and reactions

4.4.2.1 Prograde reactions

Spinel occurs frequently in the paragneisses in different assemblages. Spinel is considered as a high-temperature mineral in metamorphic rocks (Bowles et al. 2011). However, zinc increases the stability field of spinel towards lower temperatures and higher pressures (Hand et al. 1994).

In sample JU12 spinel can be found as single grain inclusions in garnet but also as small anhedral grains associated with biotite, and hematite with fine-grained ilmenite, rutile and corundum (Fig. 15). For the pure inclusions a possible reaction could be:

$$Grt + 2Sil = 3Spl + 5Qtz \quad (1)$$

i.e. an early sillimanite inclusion reacted with the garnet in response to heating or decompression (Das 2006). Although spinel-quartz assemblages are a result of metamorphism at ultra-high temperatures, a high gahnite content may allow that spinel and quartz can coexist even at temperatures corresponding to lower granulite facies (Tajčmanová et al. 2009). Spinel can also form from the breakdown of staurolite (Atkin 1978):

$$2St = 12Sil + 5Spl + Grt + 4H_2O \quad (2)$$

$$2St = 10Sil + 6Spl + Crd + 4H_2O \quad (3)$$

The association spinel-hematite-ilmenite-rutile-corundum (or -quartz) in the garnet in Fig. 15 and the assemblage in Fig. 18 could be explained by the oxidation reaction (La et al. 1987) :

$$Spl(1) + Rt + Qtz + O_2 = Spl(2) + Ilm\text{-}Hem + Crn \quad (4)$$

Sillimanite inclusions as needles in garnets are frequently observed and could have formed before or concomitantly with the garnet (McLellan 1985):

$$St + Qtz = Grt + Sil + H_2O \quad (5)$$

Related is the discontinuous reaction

$$St + Ms + Qtz = Bt + Grt + Sil + H_2O \quad (5)$$

which occurs at about 700°C and 6 kbar (McLellan 1985).

Sillimanite inclusions in garnet could also be explained by reaction (2).

Both in the cordierite-bearing rocks and the garnet-bearing sillimanite-biotite gneisses partial melting has occurred. In the garnet-bearing sillimanite-biotite gneisses this has resulted in formation of poikilitic garnet porphyroblasts in a matrix, which in some areas consists of mainly quartz and plagioclase. The formation of garnet suggests water-undersaturated melting involving breakdown of biotite according to the peritectic reaction:

$$Bt + Pl + Qtz + Sil = Grt + Kfs + L \quad (6)$$

This reaction takes place at temperatures above 650-700°C (Vernon & Clarke 2008).

Observed symplectites of biotite and plagioclase in the cordierite-bearing rocks are also indicative of melting and can be regarded as the result of the reversal of reaction (1) above; (Sawyer 2008).

4.4.2.2 Retrograde reactions

Observed foliations and lineations defined by biotite and sillimanite in Fig. 17 and Figs. 21-23, are likely the result of the breakdown of garnet and/or cordierite, i.e., the reverse of reaction (6) and:

$$Crd + Kfs + L = Sil + Bt + Qtz \quad (7)$$

Associations of sillimanite, biotite and spinel with very fine-grained staurolite and corundum (Fig. 26) could be explained by reactions like (Stoddard 1979):

$$Sil + Kfs + Rt + Spl + Grt + H_2O = St + Bt + Qtz \quad (8)$$

and

$$3Spl + 3Sil = 5Crn + Grt \quad (9)$$

The pseudomorphs after cordierite can be ascribed to a retrograde breakdown of cordierite and is commonly termed pinitization (reaction 10). Ogiermann (2003) has described different pinitization processes in detail, and distinguished four pinite types. The b-type (border) consists of muscovite and green biotite (low titanium), which form through a reaction of cordierite, K-feldspar and water:

$$Crd + Kfs + H_2O = Ms + Bt + Qtz \quad (10)$$

The m-type (mat) consists of very fine-grained aggregates of muscovite and chlorite and can also contain clays. F-type (fissure) and i-type (isotrope) pinite are enriched in Ca and can contain amorphous material. All four types can be observed in the cordierite pseudomorphs from Nygård (Fig. 13).

The muscovite-out reaction gives an upper limit of 550-650°C for the b-type pinitization and the upper stability limit for muscovite + chlorite for the m-type pinite is 500-550°C (Ogiermann 2003). Probably an external fluid is required for the supply of potassium and water for the reactions (Ogiermann 2003).

Rutile is abundant in association with ilmenite (+ quartz or corundum); it is difficult to decide if it replaces ilmenite or it is the other way round (Fig. 18). Rutile is usually indicative of medium- to high-grade metamorphism (Meinhold 2010), however, rutile can also form in low- to medium-grade metasedimentary rocks (Luvizotto et al. 2009). Rutile can also form under low-grade conditions through oxidation and metasomatism (Putnis 2009; Engvik et al. 2011):

$$Ilm \rightarrow Rt + Fe^{2+}, Fe^{3+} \quad (11)$$

where Fe is removed by fluids.

The amphibolite contains a few relicts of orthopyroxene (enstatite-hypersthene). It is not possible to decide their exact textural relationship, but they are remnants of either a primary igneous or an early high-T metamorphic assemblage. One grain looks euhedral and clear and has a partial corona of cummingtonite which clearly indicates a retrograde reaction:

$$Opx + Qtz + H_2O = Cum \quad (12)$$

4.4.2.3 Peak paragenesis

From observations above, the peak paragenesis for the paragneiss appears to be Grt + Sil + Crd + Spl + Bt + Melt + Pl + Kfs + Qtz + Ilm ± Rt ± Zrn. Remnants of prograde minerals include St, Sil, and Spl. Retrograde reactions, commonly related to deformation, caused consumption of Grt and Crd and the formation of Bt + Sil ± Ms, and later Chl + Ms. A likely peak paragenesis for the amphibolite is Grt + Hbl +Pl + Bt + Ilm ± Qtz ± Opx.

4.4.3 Mineral chemistry and zonations

The flat compositional profiles of garnet in the paragneisses reflect homogenization due to intragranular diffusion at high temperatures (>650°C) during prograde and peak regional metamorphism (Kohn 2003). The rimward increase in almandine and corresponding decrease in pyrope content is probably due to either retrograde net transfer reactions, diffusional Fe-Mg exchange during cooling, or both. Increasing Mn and Ca contents are indicative of net transfer reactions. The excess Mn and Ca will partition back into the reacting garnet during garnet consuming reaction.

A decrease in calcic content as observed for the amphibolite may be due to formation of plagioclase or amphibole in the matrix.

The zinc content of spinel in the paragneisses is remarkably high, corresponding to a gahnite content of 6 to 54%. The origin of the zinc can be in the breakdown of Zn-bearing minerals, such as biotite (Dietvorst 1980), staurolite or through desulphurisation of sphalerite (ZnS); (Bowles et al. 2011). Breakdown of Zn-bearing staurolite with X_{Zn} of about 0.18 is a likely candidate probably by a reaction similar to 2 or 3.

4.5 Thermobarometry

Almost all paragneiss samples contain the assemblage Grt + Bt + Pl + Qtz ± Sil in close contact, why this assemblage was used for P-T calculations with Win-TWQ, using the equilibria:

Zonation of minerals is in most cases insignificant,

$$\text{Prp} + \text{Ann} = \text{Alm} + \text{Phl} \quad \text{(GB thermometer)} \quad (13)$$
$$\text{Qtz} + \text{Prp} + \text{Grs} + \text{Eas} = \text{An} + \text{Phl} \quad \text{(GBPQ barometer)} \quad (15)$$
$$\text{Grs} + \text{Qtz} + \text{Sil} = \text{An} \quad \text{(GASP barometer)} \quad (14)$$

and therefore average values of microprobe traverses over the minerals were used. Average values from garnet cores were combined with average values from biotite and plagioclase grains in the matrix close to but not in contact with the garnet grain. In a few cases values from garnet rims and biotite inclusions in garnet grains were tested. A representative diagram is depicted in Fig. 29. The result for several samples is presented separately for the GB-GBPQ and the GB-GASP geothermobarometers in Table 6. For comparison the results from the calibration of the GB-GBPQ geothermobarometer according to Wu et al. (2004) with reaction (13), and the reactions

$$\text{Prp} + \text{Grs} + \text{Eas} + \text{Qtz} = \text{An} + \text{Phl} \quad (15)$$
$$\text{Alm} + \text{Grs} + \text{Sid} + \text{Qtz} = \text{An} + \text{Ann} \quad (16)$$

is also presented in Table 6. An independent test for temperature is performed with the Ti-in-biotitet geothermometer according to Henry et al. (2005) and some results for the metagneisses are also presented in Table 6. The garnet in sample JU12 contains an inclusion of spinel and corundum and therefore the assemblage Grt-Spl-Sil-Crn can be used as a geothermobarometer with the reactions:

$$\text{Alm} + \text{Crn} = \text{Sil} + \text{Hc} \quad (17)$$
$$\text{Alm} + \text{Spl} = \text{Prp} + \text{Hc} \quad (18)$$

The inclusion in sample JU12 also contains rutile, ilmenite and quartz, why the GRIPS geobarometer was tested with plagioclase close to the garnet:

$$\text{Grs} + \text{Alm} + \text{Rt} = \text{Ilm} + \text{An} + \text{Qtz} \quad (19)$$

Although the Al-in-hornblende geobarometer have been developed for granitic rocks (Anderson et al. 2008) it has been applied to mafic granulites (Ge et al. 2003) and results from the amphibolite (sample JU9B) is presented in Table 6. The hornblende-plagioclase geothermometer (Holland & Blundy 1994) was also tested for the amphibolite.

4.5.1 Results and interpretation

The results of the GB-GASP-GBPQ geothermobarometers for the paragneisses fall in the range 550-650°C and 1.5-4 kbar (Table 6). Garnet rims give somewhat lower values (450-600°C and 0.5-3 kbar) which is consistent with retrograde processes. The Ti-in-biotite

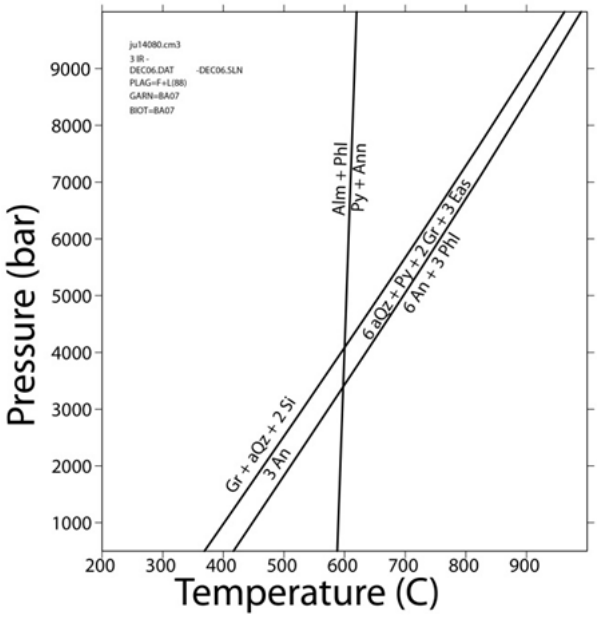

Fig. 29. P-T results from WinTWQ for fine-grained grey gneiss from Romeleklint sample JU1 site 4080 with independent reactions.

geothermometer yields higher temperatures (680-720°C), while the results from the amphibolite indicate a higher pressure (about 5 kbar). The peak parageneses (Grt + Sil + Crd + Spl + Bt + Pl + Kfs + Qtz + Ilm ± Rt ± Zrn for paragneisses JU12-14 and JU28 and Grt + Hbl + Bt + Ilm ± Qtz ± Opx for amphibolite (JU9B), together with the observed partial melting of metapelitic compositions indicate conditions at the transition between the upper amphibolite and granulite facies (650-750°C). The high temperature at the presumed peak conditions have resulted in homogenisation and eradication of any previous element zoning in the minerals, e.g. garnet and biotite. If the peak levels of e.g. Fe and Mg had been maintained, the geothermometer would indicate the peak temperature. However, during retrogression, the equilibrium composition at the mineral interfaces will change and the gradient between the rim and the interior of a grain will drive diffusion until the temperature is too low for the diffusional process (Spear 1993). For garnet the Fe/Mg ratio will increase at the rim while for biotite it will decrease for a pure exchange reaction. Diffusion in garnet is relatively slow so that a diffusion profile will be formed between the rim and the core, while for biotite diffusion is more rapid keeping biotite homogenous. Depending on the size of the garnet and the time that temperature is high enough for diffusion to act, the garnet may homogenize with a high Fe/Mg level. Higher Fe/Mg levels for garnet and lower Fe/Mg levels for biotite result in lower temperatures for the garnet-biotite geothermometer. This is likely the explanation for the observed too low temperatures. If the garnet-biotite thermometer had given higher temperatures, with the vertical line in Fig. 29 moving to the right, a higher pressure would also be the result. Although not conspicuous, some garnets show traces of retrograde net trans-

Table 6. Geothermobarometry data for paragneisses and amphibolites from Romeleåsen. C=core, M=matrix, I=inclusion, R=rim, Cl=close.

Sample	Site	Grt	Bt	Pl	Other	WinTWQ GB-GBPQ[1]		WinTWQ GB-GASP[2]		GB-GBPQ[3]		Ti-in-Bt[4]	Other	
						T(°C)	P (kbar)	T(°C)	P (kbar)	T(°C)	P (kbar)	T(°C)	T(°C)	P (kbar)
JU1	9010	C, n=6	M, n=6	M, n=6		598	1.5	602	1.7	601	3.0	714		
JU1	4080	C, n=5	M, n=5	M, n=3		598	3.4	599	4.1	616	4.1	671		
JU8A	4080	C, n=8	M, n=4	M, n=5		643	2.7	-	-	625	2.8	709		
JU11	3055	C, n=18	M, n=12	M, n=8		653	4.0	-	-	639	3.4	713		
JU12	9035	C, n=14	I, n=9	M, n=9	Spl incl	558	1.2	560	1.8	567	1.7	713	713[5]	2.9
JU12	9035	C, n=14	Cl, n=5	M, n=9	GRIPS	590	1.4	593	2.2	595	2.1	704		6.0[6]
JU12	9035	C, n=14	M, n=5	M, n=9		668	2.4	671	3.2	655	2.4	699		
JU25A1	2540	C, n=11	M, n=4	M, n=5		620	2.4	621	2.8	615	2.5	694		
JU25A1	4090	C, n=12	M, n=5	M, n=8		647	2.3	-	-	628	2.4	697		
JU25A2	9040	C, n=22	M, n=2	M, n=7		598	2.6	-	-	595	2.9	681		
JU25A2	2535	C, n=9	M, n=6	M, n=5		604	1.9	-	-	604	2.2	696		
JU25A2	2535	R, n=1	M, n=6	M, n=5		600	1.9	-	-	602	2.2	696		
JU25A2	2535	C, n=9	I, n=2	M, n=5		548	1.4	-	-	563	1.7	-		
SB1AJU	7520	C, n=9	M, n=4	M, n=2		576	0.7	582	2.2	578	1.9	683		
SB8A	8060	C, n=8	M, n=8	M, n=8		567	2.3	-	-	588	2.5	-		
SB8A	8060	R, n=2	M, n=8	M, n=8		517	3.1	-	-	538	3.3	-		
SB8A	4075	C, n=8	I, n=5	M, n=8		596	3.1	-	-	608	2.6	-		
SB8A	4075	C, n=8	M, n=3	M, n=8		560	2.6	-	-	589	2.4	-		
SB8A	4075	R, n=2	M, n=3	M, n=8		460	0.3	-	-	509	0.3	-		
JU9B	8025	C, n=8	M, n=5	M, n=4	Hbl, n=7	590[7]	5.5	-	-	-	-	-	700[8]	5.5[9]
JU9B	9060	C, n=4	M, n=1	M, n=3	Hbl, n=1	612	5.3	-	-	-	-	-	790[8]	5.6[9]
JU9B	9060	C, n=4	I, n=1	I, n=2		631	5.6	-	-	-	-	-		
JU9B	9010	C, n=4	M, n=3	M, n=2		648	5.4	-	-	-	-	-		
JU9B	1070			M, n=2	HBl, n=1								765[8]	4.8[9]

[1]P-T estimates obtained using WinTWQ with the assemblage Grt-Bt-Pl-Qtz.
[2]P-T estimates obtained using WinTWQ with the assemblage Grt-Bt-Sil-Qtz-Pl.
[3]P-T estimation obtained with the assemblage Grt-Bt-Pl-Qtz using tha calibration by Wu et al. (2004).
[4]Ti-in-Bt geothermometer by Henry et al. (2005).
[5]P-T estimation obtained using WinTWQ with the assemblage Grt-Spl-Sil-Crn.
[6]P estimation using GRIPS (Grt-Rt-Ilm-Pl-Qtz) at 700°C in WinTWQ.
[7]P-T estimation obtained using WinTWQ with the assemblage Grt-Bt-Pl-Hbl.
[8]T estimantion obtained using the HBl-Pl geothermometer (Holland & Blundy 1994) at 5.5 kbar.
[9]P estimation obtained by the Al-in-Hbl geobarometer (Lawford Anderson & Smith 1995) at 700°C.

fer reactions (increased concentrations of Fe^{2+} and Mn^{2+} at the rims). The retrograde reaction could be Grt + Kfs + $H_2O \rightarrow$ Bt + Sil + Qtz, which would result in higher Fe/Mg levels both in garnet rim and in the biotite (Spear 1993) and lead to that calculated temperatures are higher than peak temperatures (Kohn & Spear 2000).

For the amphibolite the different geobarometers yield pressures of 5-6 kbar (for the Al-in HBl geobarometer at an assumed T=700°C; the Hbl-Pl geothermometer gives much higher temperatures (700-800 °C at an assumed P=5.5 kbar) than the Grt-Bt thermometer.

The preferred interpretation of the geothermobarometry is that peak conditions have been 700°C or higher, mainly based on the Ti-in-Bt geothermometer results, and at about 5 kbar based on the WinTWQ GB -GBPQ/GB-GASP results extrapolated to 700°C, and also based on results from the amphibolite. It should, however, be noted that the prerequisite of the Ti-in-Bt geothermometer with a graphitic metapelite that restricts the amount of Fe^{3+} in the biotite, is perhaps not fulfilled, since hematite is present.

4.6 Pseudosections

Pseudosections show all the stable multivariant phase assemblages in a chosen chemical system for a specified rock composition and can be used to constrain P–T conditions and elucidate metamorphic processes. In several of the paragneisses it is evident that partial melting has occurred. The bulk composition therefore may represent the final rock composition after possible loss of the melt and the pseudosection may not be perfectly valid for the prograde evolution of the rock. Another factor that has an effect on the appearance of a pseudosection is the amount of water in the rock. During a prograde process originally hydrous mineral assemblages loose water either directly or through melting and subsequent loss of melt. If fluids are absent during the retrograde process little will happen, and the metamorphic peak will be preserved. However, if fluids are present during retrogression, rehydration will occur, leading to yet new mineral assemblages (including e.g. micas) and a bulk water content, which differs from that at the peak conditions. The bulk formulas for the studied samples contain varying amounts of water (0.5-4.2 wt-% as LOI); therefore the amount of water for the pseudosections is adjusted to

conditions of that at the vapour-saturated solidus.

Fig. 30 shows the pseudosection for the Crd-Grt bearing granofels sample JU12 in the P-T range 0.5-10 kbar and 500-900°C and melt isopleths in the range 650-800°C. In this P-T range quartz is everywhere present, rutile is present above about 8 kbar and ilmenite below this pressure range. The rock contains ilmenite, rutile and hematite and the stability field of rutile in Fig. 30 would thus indicate high pressures. The boundary for ilmenite-rutile is dependent on the oxidation status, with increasing Fe^{3+} the stability field of rutile will be displaced toward even higher pressures (Corvino et al. 2007). However, it is probable that observed rutile is due to retrograde metasomatic reactions. Staurolite can be found in the P-range 3-7 kbar and 550-650°C, however, the stability field is dependent on the amount of water. At low water content staurolite is absent, whereas at $P_{H20} = P_{TOT}$ (as expected during prograde metamorphism) the stability field of staurolite is considerably larger. Depending on the water content, chlorite is present below about 550 °C. Garnet is stable in almost the entire diagram; the lower limit depends on the amount of Mn. Cordierite is stable in the lower right corner, sillimanite in the mid to upper right corner and biotite is stable at temperatures below 750-800°C. Muscovite is stable below 600-750° C (depending on pressure) and melting starts at 650°C (higher at lower pressures). The Grt-Bt based thermobarometry result for this sample (560-670°C and 1.2-2.4 kbar) would land in the andalusite stability field, which is obviously not correct.

The appearance of the pseudosections for other samples of Crd-Grt bearing granofelses and also for the samples of Grt-Bt-Sil gneisses is broadly similar to that of sample JU12. Presence of water-bearing phases is dependent of the bulk water content.

The peak paragenesis Grt + Sil + Crd + Spl + Bt + Pl + Kfs + Qtz + Ilm is in the narrow field below the Crd-in line and the Sil-Bt-out line at 700-750°C and 3.5-5 kbar. Spinel is only stable at higher temperatures in the MnNKCFMASHT system; however the observed high content of zinc will expand the stability to

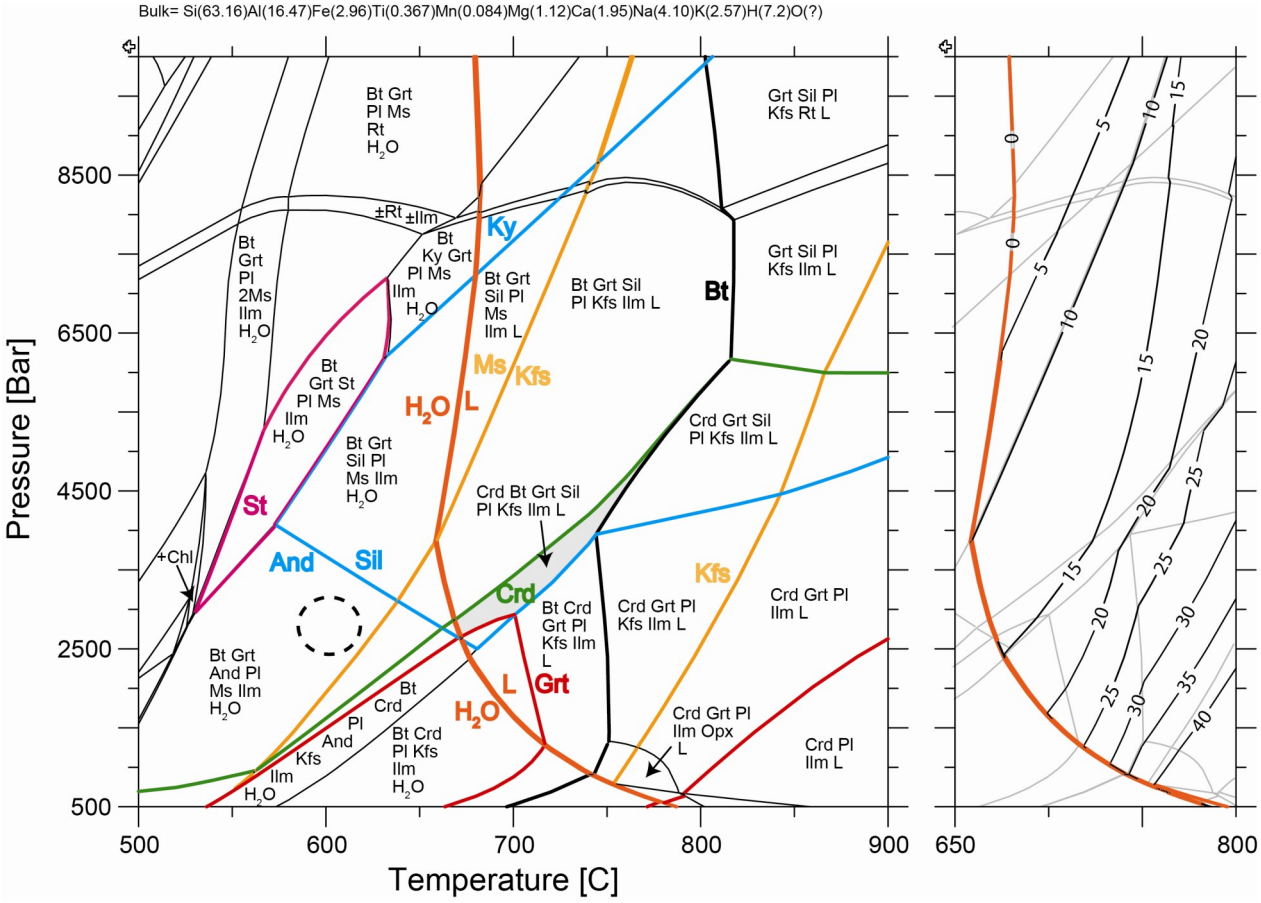

Fig. 30. P-T pseudosection for Crd-Grt-bearing granofels, sample JU12 from Nygård, calculated in the MnNKCFMASHT system with the bulk composition specified in mole proportions of elements. Assemblages for the largest fields are indicated and all fields also include quartz. The stability areas for St, Sil, Ms, Kfs, Grt, Crd, Bt, free H_2O and melt (L) are depicted with different colours. Pl is stable in the entire diagram. The stability field for staurolite is shown with pink boundaries; that of garnet with red. Cordierite is stable below the green line, sillimanite within blue lines. K-feldspar is stable between the orange lines, where the left coincides with the upper stability of muscovite. The stability fields of the peak assemblage in sample JU12 is shaded. The result for thermobarometry for sample JU12 is indicated with the hatched circle. The diagram to the right shows melt isopleths (vol%) above the solidus (orange).

lower temperatures.

Leucosome is observed in the field and melting is predicted by the pseudosection. It is generally not possible to estimate quantitatively the melt loss history, including melt amount and composition, although forward modelling has shown rather small changes on supra-solidus topologies (White & Powell 2002). To test the influence of melt reintegration, the procedure according to Indares et al. (2008) was used. The melt composition was calculated at the solidus at 680°C and 5 kbar using THERIAK. Different amounts of this composition were added to the composition of the investigated sample (JU12) and the pseudosection was recalculated. Ten percent melt reintegration did not significantly change the appearance of the pseudosection, while 20% significantly changed the fields below about 600°C, e.g. the field for staurolite disappeared. Therefore the original composition was retained for illustration of the prograde reactions.

Garnet shows almost complete homogenisation and if in equilibrium with the whole-rock composition, garnet isopleths can be used to estimate the equilibrium P and T. Three of the four end-members grow independently of each other, e.g. Ca, Mn and Fe, and should display isopleth intersections, which are clustered around the P-T point at which the garnet stabilised in composition. For sample JU12 the garnet isopleths for almandine, grossular and spessartine are plotted in Fig. 31 and the observed proportions of the end-members from Table 3 cross each other at about 725°C and 3.5 kbar, i.e. in the field for the peak paragenesis. However, for other samples tested in the same way the intersection between the three isopleths is not so well defined, indicating disequilibrium.

The pseudosections fail to explain the presence of spinel-staurolite-corundum parageneses. As mentioned before, spinel in the samples is high in zinc (gahnite), which will result in extended stability area for spinel to lower temperatures. Another suggestion is a lack of equilibrium at the thin section scale. To test this, pseudosections have been calculated for bulk compositions based on the modal proportions of minerals and their composition in parts of spinel-bearing sections where equilibrium likely has been attained. The modal proportions of the minerals within a restricted area were calculated by image analysis of the back-scattered scanning electron image, and the bulk composition was calculated from the mineral proportions and the composition of each mineral taken from SEM-analysis. An example of a pseudosection is shown in Fig. 32 where the observed paragenesis Grt-Bt-Sil-St-Spl-Crn-Ilm can be found at about 600°C and 4.5 kbar.

The pseudosection of the fine-grained dark-grey Bt-Grt gneiss sample JU26B (Fig. 33) differs from that of the other gneiss samples (Fig. 30). The pseudosection shows a mafic composition with amphibole and orthopyroxene below 5 kbar, which is in agreement with the higher content of iron and magnesium in the bulk composition and also the placing in the provenance discrimination diagram Fig. 5. However, the observed assemblage is Qtz-Pl-Bt-Grt-Opaques, which is stable in the field above 4.5-5 kbar and at temperatures of 600-750°C.

The pseudosection for the amphibolite JU9B is depicted in Fig. 34. The observed peak paragenesis Grt + Hbl + Bt + Ilm ± Qtz ± Opx can be found in the area below the solidus at about 770°C and 5.5 kbar and close to the thermobarometry results for Al-in-Hbl and Hbl-Pl. Cummingtonite and quartz can be interpreted as retrograde products during cooling from a peak 770°C and 5.5 kbar, which is at higher pressure than found for the paragneisses.

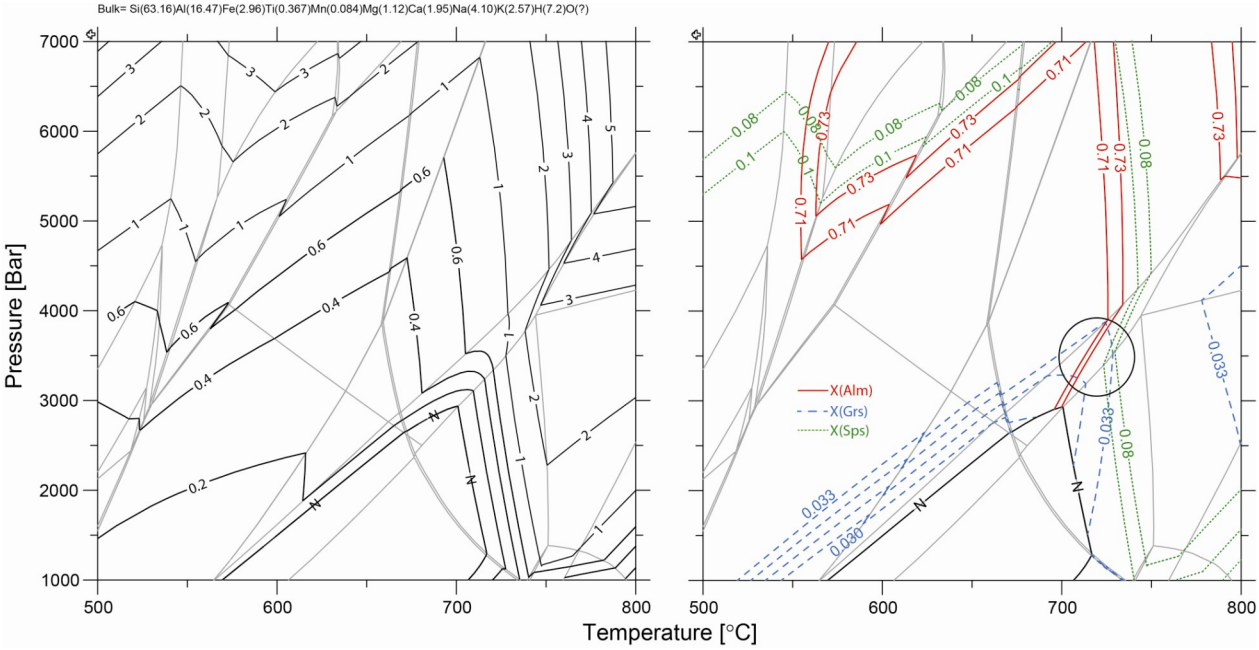

Fig. 31. Detail of Fig. 30 showing isopleths of garnet abundance (in vol%; left) and composition (XSps, XGr and XAlm; right).

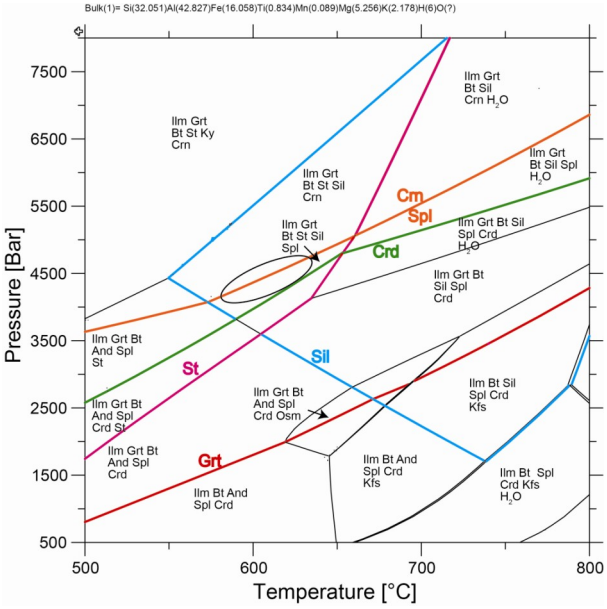

Fig. 32. Pseudosection calculated for spinel inclusion in garnet 2575 in Grt-Sil-Bt gneiss sample JU25Ab. The bulk composition was calculated from modal proportions of the minerals and their compositions determined by SEM.

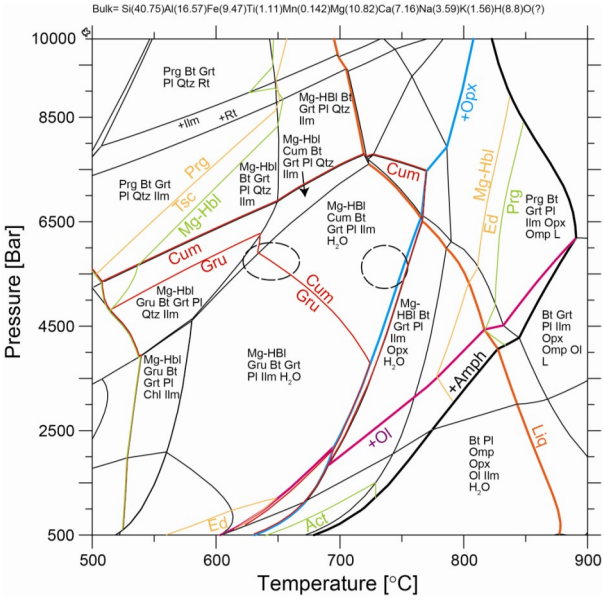

Fig. 34. Pseudosection of the amphibolite JU9B from Romeleklint. The results for thermobarometry are shown with the circle (Al-in-HBl and HBl-Pl) and ellipse (Grt-Bt-Pl-Qtz or Grt-Bt-Pl-HBl), respectively.

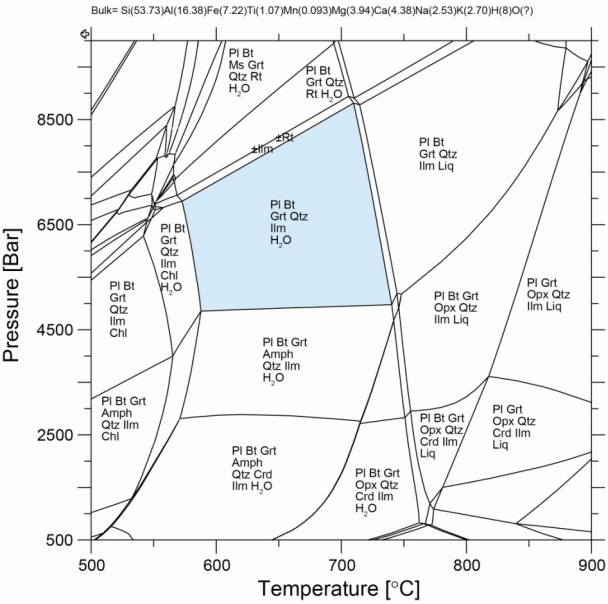

Fig. 33. Pseudosection of the fine-grained dark-grey Bt-Grt gneiss JU26B from Romeleklint.

4.7 Interpretation of P-T evolution

P-T paths are based on observed assemblages and textures in the rocks. Discussed P-T paths are depicted in Fig. 35 with numbers 1-2. A counterclock-wise path (2) is unlikely as it would pass through the andalusite stability field and not through the staurolite stability field during prograde metamorphism. Andalusite or pseudomorphs after andalusite have not been observed in the samples, although Hjelmqvist (1934) did observe andalusite in one sample from Stenberget. Observed inclusions of spinel and staurolite in garnet would also be difficult to explain since during this path garnet would decrease in modal abundance (Fig. 31) and the path would even pass through a field where garnet is absent. An isobaric temperature increase from the staurolite field is also not compatible with sillimanite inclusions in garnet; during sillimanite increase there is little change in garnet content, and during garnet increase, sillimanite will decrease.

The proposed P-T path (1) that peaks at about 750° C and about 4.5 kbar, is discussed below, including the additional reactions, which are suggested by the pseudosection (Fig. 35). Modal proportions during the path is depicted in Appendix 2.

A. Staurolite has been observed as an inclusion in garnet (sample SB6) which constrains the prograde conditions, The disappearance of staurolite from the matrix can be explained by the discontinuous reaction (5) St+Ms+Qtz=Grt+Sil+Bt+H_2O, at the boundary between the staurolite and sillimanite fields. This reaction can also explain observed sillimanite inclusions in garnet. As mentioned earlier, staurolite can break down to spinel, sillimanite, garnet or cordierite + water (reactions 2 and 3). The calculated pseudosections do not include Zn and does not show a stability field for spinel. The presence of spinel is most likely due to that small amounts of Zn has stabilized spinel at lower temperatures and/or that equilibrium was only attained in microdomains as shown above and in Fig. 32. The presence of zinc will also expand the staurolite stability field.

B. During increasing pressure and temperature the main prograde continuous reactions can be summarized as Ms+Bt+Qtz=Sil+Grt+Pl+H_2O (20), which also explains the presence of sillimanite inclusions in garnet.

C. At the wet solidus melting will start as a result of vapour-excess muscovite breakdown: Ms + Qtz + Pl + H_2O = Sil + Liq (21). Only small amounts of melt are produced (Fig. 30).

D. Further melting consumes muscovite and quartz (and garnet) under the formation of sillimanite and biotite.

E. At higher temperatures water-absent melting takes place, involving breakdown of muscovite to sillimanite and K-feldspar: Ms+Pl+Qtz=Sil+Kfs+Liq (22).

F. During decreasing pressure and increasing temperature continuous water-undersaturated melting will produce garnet (reaction 6): Bt+Pl+Qtz+Sil= Grt+Kfs+Liq.

G. Biotite and sillimanite breaks down under the formation of cordierite, potassium feldspar and melt via the reaction: Bt+Sil+Qtz+Pl=Crd+Grt+Kfs+Ilm+Liq (23). Cordierite reaches almost 8 vol% during disappearance of biotite. During cooling and decompression cordierite and K-feldspar continues to increase at the expense of garnet and sillimanite.

H. During further retrogression biotite and sillmanite are formed at the expense of garnet, cordierite and potassium feldspar. The formation of biotite and muscovite are dependent on the amount of available water, either from the melt or from external sources. In some rocks garnet and potassium feldspar formed biotite and sillimanite in association with deformation.

I. Later, cordierite undergoes further pinitisation according to reaction 10. Formation of muscovite in the pinite cannot occur until point (I) in Fig. 35.

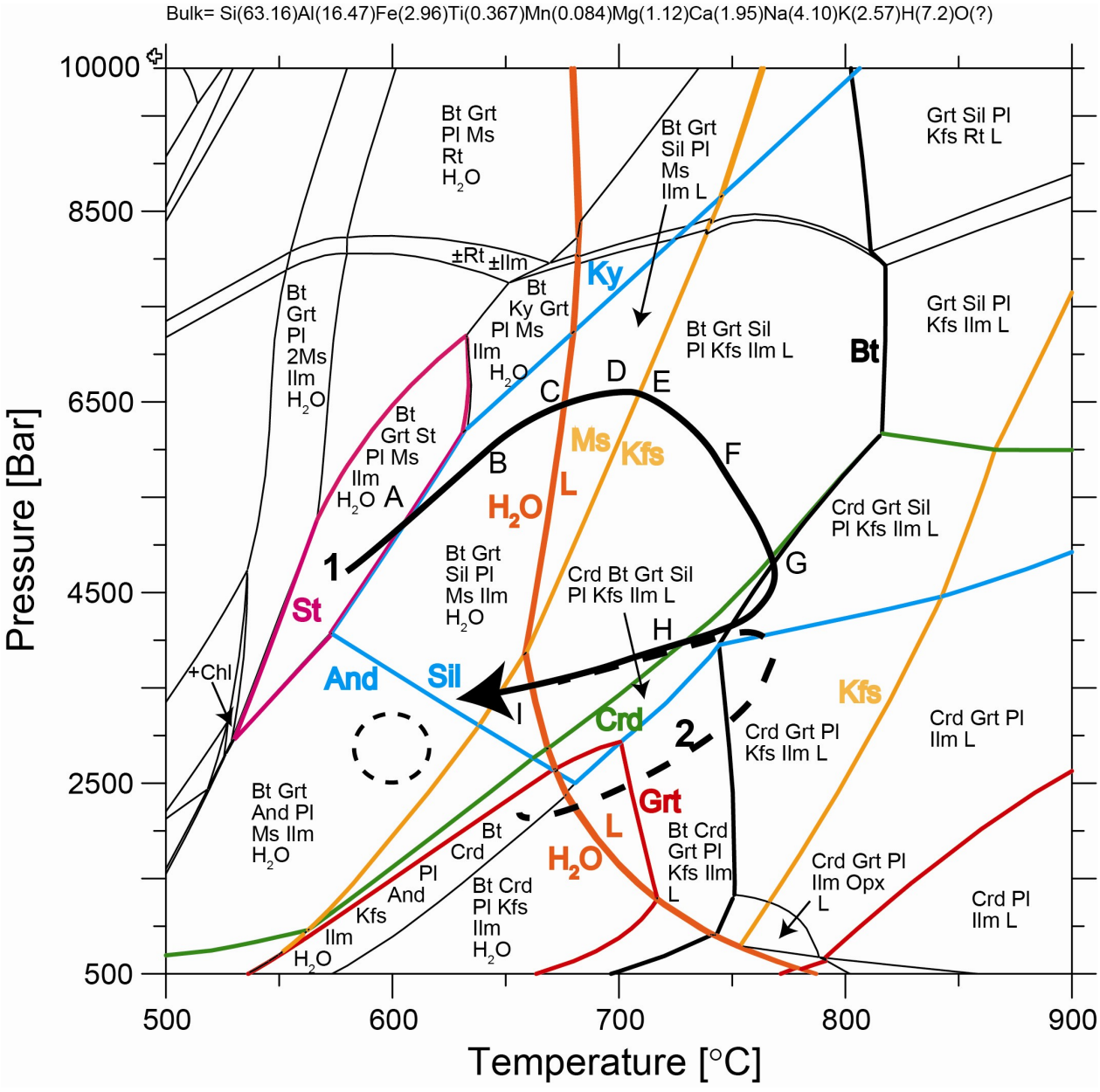

Fig. 35. Pseudosection of cordierite-sillimanite gneiss sample JU12 from Nygård with proposed P-T path discussed in the text.

During the prograde path A-G there is garnet growth (except during partial melting in the Ms-field, D) and during the retrograde path down to about 650°C garnet will be resorbed (Appendix 2), which also can be observed in higher rim concentrations of e.g. manganese for some garnets.

The mafic-like rock sample JU26B and the amphibolite sample JU9B also indicate temperatures at the peak of 700 to750°C; however at the somewhat higher pressures of 5-6 kbar.

5 Discussion

The oldest rocks of Romeleåsen may be equivalents of the TIB rocks, i.e. 1.65-1.7 Ga. Reworking probably took place at the Hallandian/Danopolian orogeny 1.47-1.38 Ga and during the Sveconorwegian orogeny 1.10-0.92 Ga. Romeleåsen was intruded by dolerite dykes around 1.2 Ga, connected to activities in the Protogine Zone, and also around 0.3 Ga connected to activities in the Tornquist Zone. Very little quantitative data is available regarding the metamorphism of Romeleåsen, but Hjelmqvist (1934) estimated the conditions to >600°C and 5-6 kbar. Petrographic studies on paragneisses in the present study show that high temperatures prevailed:

- Sillimanite is the sole alumino-silicate polymorph
- Sillimanite + K-feldspar is diagnostic of granulite facies temperatures
- Partial melting took place
- Garnet was homogenized
- Cordierite is present in melt
- Spinel is present

The findings indicate that temperatures peaked above 700°C. Though the garnet-biotite geothermometer results in temperatures at or below 600°C, these numbers are considered an artefact.. The homogenised garnets indicate that they were open to diffusion during peak temperatures. Homogenised garnets are typical at granulite-facies conditions, whereas at amphibolite-facies conditions garnets normally retain growth-zoning patterns (Frost & Chacko 1989). Although conditions are not completely fulfilled (presence of graphite) for the independent Ti-in-biotite geothermometer, temperatures in the range 680-720°C are obtained. If a temperature of 700°C is used for extrapolation of the GBPQ or GASP barometer, a pressure above 5 kbar is obtained, which is in agreement with the results from the Al-in-Hbl barometer.

Pseudosection modelling is recognised as powerful method, which allows the observed assemblage to be quantitatively constrained for a specified rock composition. A P-T evolution can be deduced through the interpreted textural evolution of the rock (Powell & Holland 2008). The peak paragenesis for the paragneisses is restricted to an area corresponding to 700-750°C and 3.5-5 kbar, while for the amphibolite the peak paragenesis can be found at about the same temperatures but somewhat higher pressures. For the Crd-Grt bearing paragneisses the formation of pseudomorphs after cordierite with Bt-Sil-Ms points to a decreasing temperature with supply of external fluids and possibly decreasing pressure (Fig. 35). The prograde path to the observed peak conditions is indeed difficult to discern; it could be clockwise or counterclockwise. A clockwise path is inferred because:

- a counterclockwise path would pass almost entirely through the andalusite field, and there are no remains or pseudomorphs after andalusite
- inclusions of staurolite have been found in garnet, and at a counterclockwise path garnet would initially decrease in abundance or even disappear

The proposed shape with temperature increase after the peak pressure is mainly based on that:

- sillimanite can form inclusions in garnet only during a concurrent pressure and temperature increase (modal increase of both sillimanite and garnet).
- the temperature peak is in the stability field of cordierite

With a temperature higher than 750°C biotite would disappear, and observed biotite would be retrograde. It is difficult to decide how much of the biotite that is retrograde, but it could have contributed to the deviating geothermometry.

Path 1 in Fig. 35 is in agreement with burial and subsequent exhumation of middle crust at collision with a temperature increase after the peak pressure cf. Thompson & England (1984). If peak metamorphism is constrained to 5 kbar and 750°C, this corresponds to an average geothermal gradient of about 40°C/km (assuming 1kbar=3.5 km rock pile). An assumed peak pressure of 6.5 kbar at about 700°C corresponds to a geothermal gradient of about 30°C/km. The high T/P environment can be explained by coeval magmatism. The conditions are in agreement with an accretionary orogenic setting.

The Crd-bearing granofelses from Nygård show almost no deformation, while paragneisses from Romeleklint and Stenberget are heterogeneously deformed. The pseudosections for most paragneisses are similar, so if they have been exposed to the same conditions, they should contain the same assemblages. It is most likely that all parageneses had the assemblage Crd-Grt as for Nygård at peak conditions, and that the (Grt)-Sil-Bt assemblages reflect re-equilibration during early retrogression.

Which of the two orogenies (Hallandian/ Danopolonian or Sveconorwegian) that is responsible for the metamorphic stages (A)-G, and H respectively, is yet unknown. The paragneisses contain abundant large zircons and some monazite. The high closure temperatures of these minerals make them suitable for dating metamorphic events at upper amphibolite and granulite facies (Hermann & Rubatto 2003) and could be subject for a rewarding future study.

6 Conclusions

By a combination of petrography, geothermobarometry and use of pseudosections it is concluded that:

- rocks of the middle part of the horst Romeleåsen have undergone metamorphism at upper amphibolite to granulite conditions peaking at about 750°C and 4-5 kbar.
- The rocks underwent a clockwise path with burial and exhumation during a collisional event.

To assign the metamorphism to either the Hallandian/Danopolonian or the Sveconorwegian orogeny, dating of zircons that are abundant in the paragneisses could be tested.

7 Acknowledgements

First of all thanks to Lotta Möller for introducing me to the fascinating subject of rock metamorphism and for suggesting to apply this on 'doorstep'-rocks. Also thanks to Leif Johansson and Ulf Söderlund for help with all practicalities with dividing rocks in their constituent parts and for help with instruments for observing and measuring these parts.

This MSc project forms a part of the project "Pressure-Temperature-time evolution across the southernmost part of the Protogine Zone, Skåne, south Sweden" and was financially supported by Kungliga Fysiografiska Sällskapet, through a grant to C. Möller. In addition, it is an integral part of the project Metamorphic Map of Sweden (granted by SGU to A. Skelton, Stockholm University) with the aim of compiling P-T-t data towards building a metamorphic map of Sweden. Hugo Wikman and Karl-Axel Kornfeldt introduced J. Andersson and C. Möller to the geology of horst Romeleåsen, under superb guiding.

8 References

Anderson, J.L., Barth, a. P., Wooden, J.L. & Mazdab, F., 2008: Thermometers and Thermobarometers in Granitic Systems. *Reviews in Mineralogy and* Geochemistry 69, 121–142.

Appelquist, K., 2010: *Proterozoic crustal evolution in southcentral Fennoscandia*. Ph.D.thesis, University of Gothenburg, Gothenburg, Sweden, 39 pp.

Atkin, B.P., 1978: Hercynite as a breakdown product of staurolite from within the aureole of the Ardara Pluton , Co. Donegal , Eire. *Mineralogical Magazine 42*, 237–9.

Bergerat, F., Angelier, J. & Andreasson, P.-G., 2007: Evolution of paleostress fields and brittle deformation of the Tornquist Zone in Scania (Sweden) during Permo-Mesozoic and Cenozoic times. *Tectonophysics 444*, 93–110.

Berman, R.G. & Aranovich, L.Y., 1996: Optimized standard state and solution properties of minerals. I. Model calibration for olivine, orthopyroxene, cordierite, garnet, and ilmenite in the system FeO-MgO-CaO-Al2O3-TiO2-SiO2. *Contributions to Mineralogy and Petrology 126*, 1–24.

Berman, R.G., 1988: Internally-Consistent Thermodynamic Data for Minerals in the System Na2O-K2O-CaO-MgO-FeO-Fe2O3-Al2O3-SiO2-TiO2-H2O-CO2. *Journal of Petrology 29*, 445–522.

Berman, R.G., 1991: Thermobarometry using multi-equilibrium calculations: a new technique, with petrological applications. *Canadian Mineralogist 29*, 833–855.

Berman, R.G., 2007: winTWQ (version 2.3): a software package for performing internally-consistent thermobarometric calculations. *Geological Survey of Canada open file 5462*.

Bingen, B., Andersson, J., Söderlund, U. & Möller, C., 2008a: The Mesoproterozoic in the Nordic countries. *Episodes 31*, 29–34.

Bingen, B., Nordgulen, Ø. & Viola, G., 2008b: A four-phase model for the Sveconorwegian orogeny , SW Scandinavia. *Norwegian Journal of Geology 88*, 43–72.

Bogdanova, S.V., Bingen, B., Gorbatschev, R., Kheraskova, T.N., Kozlov, V.I., Puchkov, V.N. & Volozh, Y.A., 2008: The East European Craton (Baltica) before and during the assembly of Rodinia. *Precambrian Research 160*, 23–45.

Bowles, J.F.W., Howie, R.A., Vaughan, D.J. & Zussman, J., 2011: Non-silicates: Oxides, Hydrooxides and Sulphides. *In* (Deer, Howie, R.A. & Zussman, J., eds.): *Rock-forming Minerals Volume 5A*. The Geological Society, Bath, p. 927.

Brander, L., 2011: *The Mesoproterozoic Hallandian event - a region-scale orogenic event in the Fennoscandian Shield*. Ph.D. thesis, University of Gothenburg, Gothenburg, Sweden. 24 pp.

Brueckner, H.K., 2009: Subduction of continental crust, the origin of post-orogenic granitoids (and anorthosites?) and the evolution of Fennoscandia. *Journal of the Geological Society 166,* 753–762.

de Capitani, C. & Petrakakis, K., 2010: The computation of equilibrium assemblage diagrams with Theriak/Domino software. *American Mineralogist 95*, 1006–1016.

de Capitani, C., 2012: THERIAK-DOMINO http://titan.minpet.unibas.ch/minpet/theriak/theruser.html. 20 November 2012.

Cederberg, J., 2011: *U-Pb baddelyit dateringar av basiska gångar längs Romeleåsen i Skåne och deras påverkan av plastisk deformation i Protoginzonen*. Thesis, University of Lund, Lund, Sweden. 16 pp.

Coggon, R., Holland, T.J.B. & Street, D., 2002: Mixing properties of phengitic micas and revised garnet-phengite thermobarometers. *Journal of Metamorphic Geology 20*, 683–696.

Corvino, A.F., Boger, S.D. & Wilson, C.J.L., 2007: Metamorphic conditions during formation of a metapelitic sillimanite-garnet gneiss from Clemence Massif , Prince Charles Mountains , East Antarctica. *In* (Cooper, A.K. & Raymond, C.R., eds): *Antarctica: A Keystone in a Changing World - Online Proceedings of the 10th ISAES. USGS Open-File Report 2007-1047, Short Research Paper 062.* 9pp.

Dachs, E. & Geiger, C.A., 2007: Entropies of mixing and subsolidus phase relations of forsterite-fayalite

(Mg2SiO4-Fe2SiO4) solid solutions. *American Mineralogist 92,* 699–702.

Das, K., 2006: Garnet-spinel intergrowths in ultrahigh-temperature granulite, Eastern Ghats, India: Possible evidence of an early Tschermak-rich orthopyroxene during prograde metamorphism. *American Mineralogist 91,* 375–384.

Diener, J.F.A., Powell, R., White, R.W. & Holland, T.J.B., 2007: A new thermodynamic model for clino- and orthoamphiboles in the system Na2O-CaO-FeO-MgO-Al2O3-SiO2-H2O-O. *Journal of Metamorphic Geology 25*, 631–656.

Dietvorst, E.J.L., 1980: Biotite Breakdown and the Formation of Gahnite in Metapelitic Rocks from Kemiö, Southwest Finland. *Contributions to Mineralogy and Petrology 75*, 327–337.

Engvik, a. K., Mezger, K., Wortelkamp, S., Bast, R., Corfu, F., Korneliussen, a., Ihlen, P., Bingen, B. & Austrheim, H., 2011: Metasomatism of gabbro - mineral replacement and element mobilization during the Sveconorwegian metamorphic event. Journal of Metamorphic Geology, 29, 399–423.

Erlström, M., Sivhed, U., Wikman, H. & Kornfält, K.-A., 2004: *Beskrivning till berggrundskartorna 2D Tomellilla NV, NO, SV, SO; 2E Simrishamn NV, SV; 1D Ystad NV, NO; 1E Örnahusen NV. Af 212-214.* Sveriges geologiska undersökning, Uppsala. 141 pp.

Erlström, M., Thomas, S.A., Deeks, N. & Sivhed, U., 1997: Structure and tectonic evolution of the Tornquist Zone and adjacent sedimentary basins in Scania and the southern Baltic Sea area. *Tectonophysics 271,* 191–215.

Frost, B.R. & Chacko, T., 1989: The granulite uncertainty principle: limitations on thermobarometry in granulites. *The Journal of Geology 97*, 435–450.

Ge, W., Zhao, G., Sun, D., Wu, F. & Lin, Q., 2003: Metamorphic P-T Path of the Southern Jilin Complex : Implications for Tectonic Evolution of the Eastern Block of the North China Craton. *International Geology Review 45,* 1029–1043.

Giere, R., Rumble, D., Gunther, D., Connolly, J. & Caddick, M.J., 2011: Correlation of Growth and Breakdown of Major and Accessory Minerals in Metapelites from Campolungo, Central Alps. *Journal of Petrology 52*, 2293–2334.

Green, E., Holland, T. & Powell, R., 2007: An order-disorder model for omphacitic pyroxenes in the system jadeite-diopside-hedenbergite-acmite, with applications to eclogitic rocks. *American Mineralogist 92,* 1181–1189.

Hand, M., Scrimgeour, I., Powell, R., Stuwe, K. & Wilson, C.J.L., 1994: Metapelitic granulites from Jetty Peninsula , east Antarctica : formation during a single event or by polymetamorphism ? *Journal of Metamorphic Geology 12,* 557–573.

Henry, D.J., Guidotti, C. V. & Thomson, J.A., 2005: The Ti-saturation surface for low-to-medium pressure metapelitic biotites: Implications for geothermometry and Ti-substitution mechanisms. *American Mineralogist 90*, 316–328.

Hermann, J. & Rubatto, D., 2003: Relating zircon and monazite domains to garnet growth zones: age and duration of granulite facies metamorphism in the Val Malenco lower crust. *Journal of Metamorphic Geology 21*, 833–852.

Herron, M.M., 1988: Geochemical classification of terrigenous sands and shales from core or log data. Journal Sedimentary *Petrology 58,* 820–829.

Hjelmqvist, S., 1934: Zur Geologie des Sudschwedischen Grundgebirges. Die Kristallinischen Gesteine des Romeleåaen. *Meddelande från Lunds Geologisk-Mineralogiska Institution 58*, 183pp.

Holland, T. & Blundy, J., 1994: Non-ideal interactions in calcic amphiboles and their bearing on amphibole-plagioclase thermometry. *Contributions to Mineralogy and Petrology 116*, 433–447.

Holland, T. & Powell, R., 2003: Activity-composition relations for phases in petrological calculations: an asymmetric multicomponent formulation. *Contributions to Mineralogy and Petrology 145*, 492–501.

Holland, T., 2012: *AX. A program to calculate activities of mineral endmembers from chemical analyse*. https://publications.esc.cam.ac.uk/research/research-groups/holland/ax. 20 November 2012.

Holland, T.J.B., Baker, J.M. & Powell, R., 1998: Mixing properties and activity-composition relationships of chlorites in the system MgO-FeO-Al2O3-SiO2-H2O. *European Journal of Mineralogy 10*, 395–406.

Holland, T.J.B. & Powell, R., 1998: An internally consistent thermodynamic data set for phases of petrological interest. Journal of Metamorphic *Geology 16,* 309–343.

Högdahl, K., Andersson, U.B. & Eklund, O., 2004: The Transscandinavian Igneous Belt (TIB) in Sweden : a review of its character and evolution. *Geological Survey of Finland, Special Paper 37*, 125 pp.

Indares, A., White, R.W. & Powell, R., 2008: Phase equilibria modelling of kyanite-bearing anatectic paragneisses from the central Grenville Province. Journal of Metamorphic *Geology 26*, 815–836.

Johansson, A., Meier, M., Oberli, F. & Wikman, H., 1993: The early evolution of the Southwest Swedish Gneiss Province : geochronological and isotopic evidence from southernmost Sweden. *Precambrian Research 64*, 361–388.

Kohn, M.J. & Spear, F., 2000: Retrograde net transfer reaction insurance for pressure-temperature estimates. *Geology 28*, 1127–1130.

Kohn, M.J., 2003: Geochemical Zoning in Metamorphic Minerals. *In* (Rudnick, R., ed.) : *The Crust. Treatise on Geochemistry Volume 3* Elsevier, Amsterdam, pp. 229–261.

La, R.K., Ackermand, D. & Upadhyay, H., 1987: P-T-X Relationships Deduced from Corona Textures in Sapphirine-Spinel-Quartz Assemblages from Paderu, Southern India. *Journal of Petrology 28*, 1139–

1168.
Lawford Anderson, J. & Smith, D.R., 1995: The effects of temperature and fO2 on the Al-in-hornblende barometer. *American Mineralogist 80*, 549–559.
Luvizotto, G.L., Zack, T., Triebold, S. & Eynatten, H., 2009: Rutile occurrence and trace element behavior in medium-grade metasedimentary rocks: example from the Erzgebirge, Germany. *Mineralogy and Petrology 97,* 233–249.
Mahar, E.M., Baker, J.M., Powell, R., Holland, T.J.B. & Howell, N., 1997: The effect of Mn on mineral stability in metapelites. *Journal of Metamorphic Geology 15*, 223–238.
McLellan, E., 1985: Metamorphic Reactions in the Kyanite and Sillimanite Zones of the Barrovian Type Area. *Journal of Petrology 26*, 789–818.
Meinhold, G., 2010: Rutile and its applications in earth sciences. *Earth-Science Reviews 102*, 1–28.
Möller, C., Andersson, J., Lundqvist, I. & Hellström, F., 2007: Linking deformation, migmatite formation and zircon U-Pb geochronology in polymetamorphic orthogneiss, Sveconorwegian Province, Sweden. *Journal of Metamorphic Geology 25*, 727–750.
Ogiermann, J.C., 2003: *Cordierite and its retrograde breakdown products as monitors of fluid-rock interaction during retrograde path metamorphism: Case studies in the Schwarzwald and the Bayerische Wald (Variscan belt, Germany).* Ph.D. thesis, Ruperto-Carola University of Heidelberg, Heidelberg, Germany. 199 pp.
Powell, R. & Holland, T., 1999: Relating formulations of the thermodynamics of mineral solid solutions: Activity modeling of pyroxenes, amphiboles, and micas. *American Mineralogist 84*, 1–14.
Powell, R. & Holland, T., 2012: THERMOCALC. http://www.metamorph.geo.uni-mainz.de/thermocalc/index.html. 20 November 2012.
Powell, R. & Holland, T.J.B., 2008: On thermobarometry. *Journal of Metamorphic Geology 26*, 155–179.
Putnis, a., 2009: Mineral Replacement Reactions. Reviews in Mineralogy and Geochemistry, 70, 87–124.
Rieuwers, M.T., 2010: *Integrating microstructure and geothermobarometry in deciphering complex tectonometamorphic histories : examples from the New England Appalachians.* Ph.D. thesis, James Cook University, Townsville, Australia. 189 pp.
Roser, B.P. & Korsch, R.J., 1986: Determination of tectonic setting of sandstone-mudstone suite using SiO2 content and K2O/Na2O ratio. *Journal of Geology 94,* 635–650.
Roser, B.P. & Korsch, R.J., 1988: Provenance signatures of sandstonr-mudstone suites determined using discriminant function analysis of major-element data. *Science 67*, 119–139.
Sawyer, E.W., 2008: *Atlas of Migmatites*. National Research Council of Canada. 369 pp.
Sivhed, U., Wikman, H. & Erlström, M., 1999: *Beskrivning till berggrundskartorna 1C Trelleborg NV and NO; 2C Malmö SV, SO, NV and NO. Af 191-194.* Sveriges geologiska undersökning, Uppsala. 143 pp.
Spear, F.S., 1993: *Metamorphic Phase Equilibria and Pressure-Temperature-Time Paths*. Mineralogical Society of America, Washington. 700pp.
Stoddard, E.F., 1979: Zinc-rich hercynite in high-grade metamorphic rocks : a product of the dehydration of staurolite. *American Mineralogist 64*, 736–741.
Söderlund, U., Karlsson, C., Johansson, L. & Larsson, K., 2008: The Kullaberg peninsula – a glimpse of the Proterozoic evolution of SW Fennoscandia. *GFF 130*, 1–10.
Tajčmanová, L., Konopásek, J. & Košler, J., 2009: Distribution of zinc and its role in the stabilization of spinel in high-grade felsic rocks of the Moldanubian domain (Bohemian Massif). *European Journal of Mineralogy 21,* 407–418.
Thompson, B. & England, P.C., 1984: Pressure-Temperature-Time Paths of Regional Metamorphism II . Their Inference and Interpretation using Mineral Assemblages in Metamorphic Rocks, *Journal of Petrology 25*, 929–955.
Vance, D. & Holland, T., 1993: A detailed isotopic and petrological study of a single garnet from the Gassetts Schist, Vermont. *Contributions to Mineralogy and Petrology 114,* 101–118.
Vernon, R.H. & Clarke, G.L., 2008: *Principles of Metamorphic Petrology.* Cambridge University Press, New York. 446 pp.
Vernon, R.H., 1987: Growth and concentration of fibrous sillimanite related to heterogeneous deformation in K-feldspar-sillimanite metapelites. *Journal of Metamorphic Geology 5*, 51–68.
White, R.W., Powell, R. & Clarke, G.L., 2002: The interpretation of reaction textures in Fe-rich metapelitic granulites of the Musgrave Block, central Australia : constraints from mineral equilibria calculations in the system K2O-FeO-MgO-Al2O3-SiO2-H2O-TiO2-Fe2O3. *Journal of Metamorphic Geology 20*, 41–55.
White, R.W., Powell, R. & Holland, T.J.B., 2007: Progress relating to calculation of partial melting equilibria for metapelites. *Journal of Metamorphic Geology 25*, 511–527.
White, R.W. & Powell, R., 2002: Melt loss and the preservation of granulite facies mineral assemblages. Journal of *Metamorphic Geology 20,* 621–632.
Wood, B.J., Hackler, R.T. & Dobson, D.P., 1994: Experimental determination of Mn-Mg mixing properties in garnet, olivine and oxide. *Contributions to Mineralogy and Petrology 115,* 438–448.
Wu, C.-M., Zhang, J. & Ren, L.-D., 2004: Empirical Garnet-Biotite-Plagioclase-Quartz (GBPQ) Geobarometry in Medium- to High-Grade Metapelites. *Journal of Petrology 45*, 1907–1921.

9 Appendices

Appendx 1. Solution models used for Theriak-Domino pseudosection construction

Mineral	Model	Reference
Garnet	Ideal mixing of Alm-Prp-Grs-Spss on a ternary site with Margules terms (kJ/mole) W_{Prp-Gr}=33, $W_{Alm-Prp}$=2.5, $W_{Prp-Spss}$=4.5, $W_{Alm-Spss}$=0.24	(Vance & Holland 1993) (Holland & Powell 1998) (Wood et al. 1994) (Rieuwers 2010)
Feldspar	Asymmetrical ideal mixing of San, Ab (α=0.643) and An on a single site with Margules terms W_{Ab-An}=3.1, W_{Ab-San}=25.1-0.0108T+0.343, W_{San-An}=40	(Holland & Powell 2003)
Ilmenite	Ideal mixing of Ilm-Geikelite-Pyrophanite	
Orto-pyroxenes	Ideal mixing of Mg and Fe between two sites (En=Mg-Mg, Fs=Fe-Fe, FMpyx=Fe-Mg and MgTscherpyx=Mg-Al)) with Margules terms W_{En-Fs}=6.8, $W_{En-FMpyx}$=4.5, $W_{Fs-FMpyx}$=4.5, $W_{Fs-MgTscherpyx}$=-1.0, $W_{FMpyx-Mg-Tscerpyx}$=1.2	(Powell & Holland 1999)
Clino-pyroxenes	Ideal mixing on 2 sites: M1a(2):Ca,Mg,Fe,Al – M1b(2):Ca,Mg,Fe,Al. Di:Ca,Mg-Ca,Mg, Jd:Al,Al-Al,Al, Hd:Ca,Fe-Ca,Fe, Omp:Al,Al-Ca,Mg. Margules terms: W_{Di-Jd}=26.0, W_{Omp-Jd}=16.0, W_{Omp-Di}=16.0, W_{Omp-Hd}=17.0, W_{Hd-Jd}=24.0, W_{Di-Hd}=4.0	(Green et al. 2007)
Chloritoid	Ideal mixing of Mg, Fe and Mn on a single site with Margules terms W_{Mg-Fe}=1.0	(Holland & Powell 1998)
Chlorite	Ideal mixing on 4 sites : M23(4): Mg,Fe,Mn, M1(1):Mg,Fe,Al,Mn, M4(1): Mg,Al,Fe,Mn, T1(2):Si;Al. Al-free-chlorite: Mg,Mg,Mg,Mg-Mg-Mg-Si,Si, clinochlore: Mg,Mg,Mg,Mg-Mg-Al-Al,Si, daphnite: Fe,Fe,Fe,Fe-Fe-Al-Al,Si, amesite: Mg,Mg,Mg,Mg-Al-Al-Al,Al, Mn-chlorite: Mn,Mn,Mn,Mn-Mn-Mn-Al,Si. Margules terms: $W_{Al-free-chlorite-clonochlore}$=18.0, $W_{Al-free-chlorite-daphnite}$=14.5, $W_{Al-free-chlorite-amesite}$=20.0, $W_{clinochlore-daphnite}$=2.5, $W_{clinochlore-amesite}$=18.0, $W_{daphnite-amesite}$=13.5	(Holland et al. 1998)
White mica	Asymmetrical ideal mixing on 3 sites: A(1):K,Na, M2A(1):Al,Mg,Fe, T1(2):Al,Si. Ms (α=0.63):K-Al-Al,Si, Cel (α=0.63): K-Mg-Si,Si, Fe-Cel (α=0.63): K-Fe-Si,Si, Pg (α=0.37): Na-Al-Al,Si. Margules terms: W_{Ms-Pg}=10.12+0.0034T+0.353P, W_{Ms-Cel}=0.2P, $W_{Ms-Fe-Cel}$=0.2P, W_{Pg-Cel}=52.0, $W_{Pg-Fe-Cel}$=52.0	(Coggon et al. 2002)
Biotite	Ideal mixing on 4 sites: M1(1):Mg,Fe,Al,Ti, M2(2):v,Mg,Fe,Mn, T1(2):Si,Al, V (2):OH,O. Phl: Mg-Mg,Mg-Al,Si,-OH,OH, Ann: Fe-Fe,Fe-Al,Si-OH,OH, oBt:Fe-Mg,Mg-Al,Si-OH,OH, East:Al,Mg,Mg-Al,Al,-OH,OH, tBt:Ti-Mg,Mg-Al,Si-O,O. Margules terms: $W_{Phl-Ann}$:9.0, $W_{Phl-oBt}$=3.0, $W_{Phl-East}$:10.0, $W_{Ann-oBt}$:6.0, $W_{Ann-East}$=-1.0, $W_{Ann-tBt}$=10.0, $W_{oBt-East}$=10.0.	(White et al. 2007)
Staurolite	Ideal mixing of Mg, Fe and Mn on a quadruple site with the Margules term $W_{Mg\_St-Fe\_St}$=-8.0	(Mahar et al. 1997)
Cordierite	Ideal mixing of Fe, Mg and Mn on a binary site + hydrous Crd	(Holland & Powell 1998)
Spinel	Ideal mixing on two sites: A(1):Al,Ti-B(1):Mg,Fe. Spl: Al-Mg, Herc: Al-Fe, Usp: Ti-Fe. Margules terms: W_{HcUsp}=27.0, $W_{Spl-Usp}$=30.00	(White et al. 2002)
Clino-amphiboles	Asymmetrical mixing on 5 sites: A(1):v,Na – M1(3):Mg,Fe – M2(2): Mg,Al,Fe – M4 (2):Ca,Na,Mg,Fe – T(4):Si,Al. Tr(α=1.0): v-Mg,Mg,Mg-Mg,Mg-Ca,Ca-Si,Si,Si,Si, Ts (α=1.5): v-Mg,Mg,Mg-Al,Al-Ca,Ca-Si,Si,Al,Al, Prg(α1.7): Na-Mg,Mg,Mg-Mg,Al-Ca,Ca-Si,Si,Al,Al, Gln(α=0.8): v-Mg,Mg,Mg-Al,Al-Na,Na-Si,Si,Si,Si, Cum(α=1.0): v-Mg,Mg,Mg-Mg,Mg-Mg,Mg,-Si,Si,Si,Si, Gru(α=1.0):v-Fe,Fe,Fe-Fe,Fe-Fe,Fe-Si,Si,Si,Si, acam(α=1.0): v-Mg,Mg,Mg-Fe,Fe-Fe,Fe-Si,Si,Si,Si, bcam(α=1.0): v-Fe,Fe,Fe-Mg,Mg-Fe,Fe-Si,Si,Si,Si. Margules terms: W_{Tr-Ts}=20.0, W_{Tr-Prg}=25.0, W_{Tr-Gln}=65.0, W_{Tr-Cum}=45.0, W_{Tr-Gru}=75.0, $W_{Tr-acam}$=57.0, $W_{Tr-bcam}$=63.0, W_{Ts-Prg}=-40.0, W_{Ts-Gln}=25.0, W_{Ts-Cum}=70.0, W_{Ts-Gru}=80.0, $W_{Ts-acam}$=70.0, $W_{Ts-bcam}$=72.5, $W_{Prg-Gln}$=50.0, $W_{Prg-Cum}$=90.0, $W_{Prg-Gru}$=106.7, $W_{Prgacam}$=94.8, $W_{Prg-bcam}$=94.8, $W_{Gln-Cum}$=100.0, $W_{Gln-Gru}$=113.5, $W_{Gln-acam}$=100.0, $W_{Gln-bcam}$=111.2, $W_{Cum-Gru}$=33.0, $W_{Cum-acam}$=18.0, $W_{Cum-bcam}$=23.0, $W_{Gru-acam}$=12.0, $W_{Gru-bcam}$=8.0, $W_{acam-bcam}$=20.0	(Diener et al. 2007)
Olivine	Ideal mixing of Fe and Mg on a binary site. Fa:Fe,Fe, Fo:Mg,Mg with Margules terms W_{Fo-Fa}=10.6-0.0016T	(Dachs & Geiger 2007)
Melt	Mixing of qtzliq-abliq-kspliq-anliq-silliq-foliq-faliq-h2oliq with Margules terms $W_{qtzliq-abliq}$=12.0-0.40P, $W_{qtzliq-ksp-liq}$=-2.0-0.50P, $W_{qtzliq-anliq}$=-10.0, $W_{qtzliq-silliq}$=12.00, $W_{qtzliq-foliq}$=12.0-0.40P, $W_{qtzliq-faliq}$=14.0, $W_{qtzliq-h2oliq}$=15.0, $W_{abliq-kspliq}$=-6.0+3.0P, $W_{abliq-silliq}$=12.0, $W_{abliq-foliq}$=10.0, $W_{abliq-faliq}$=2.0, $W_{abliq-h2oliq}$=1.0-0.2P, $W_{anliq-h20liq}$=9.0-0.85P, $W_{silliq-foliq}$=12.0, $W_{silliq-faliq}$=12.0, $W_{silliq-h2oliq}$=16.0, $W_{foliq-faliq}$=18.0, $W_{foliq-h2oliq}$=11.0-0.50P, $W_{faliq-h2oliq}$=12.0	(White et al. 2007)

Appendix 2. Proposed P-T path 1 in Fig. 35 with the steps indicated with capital letters. Vertical scale: vol%.

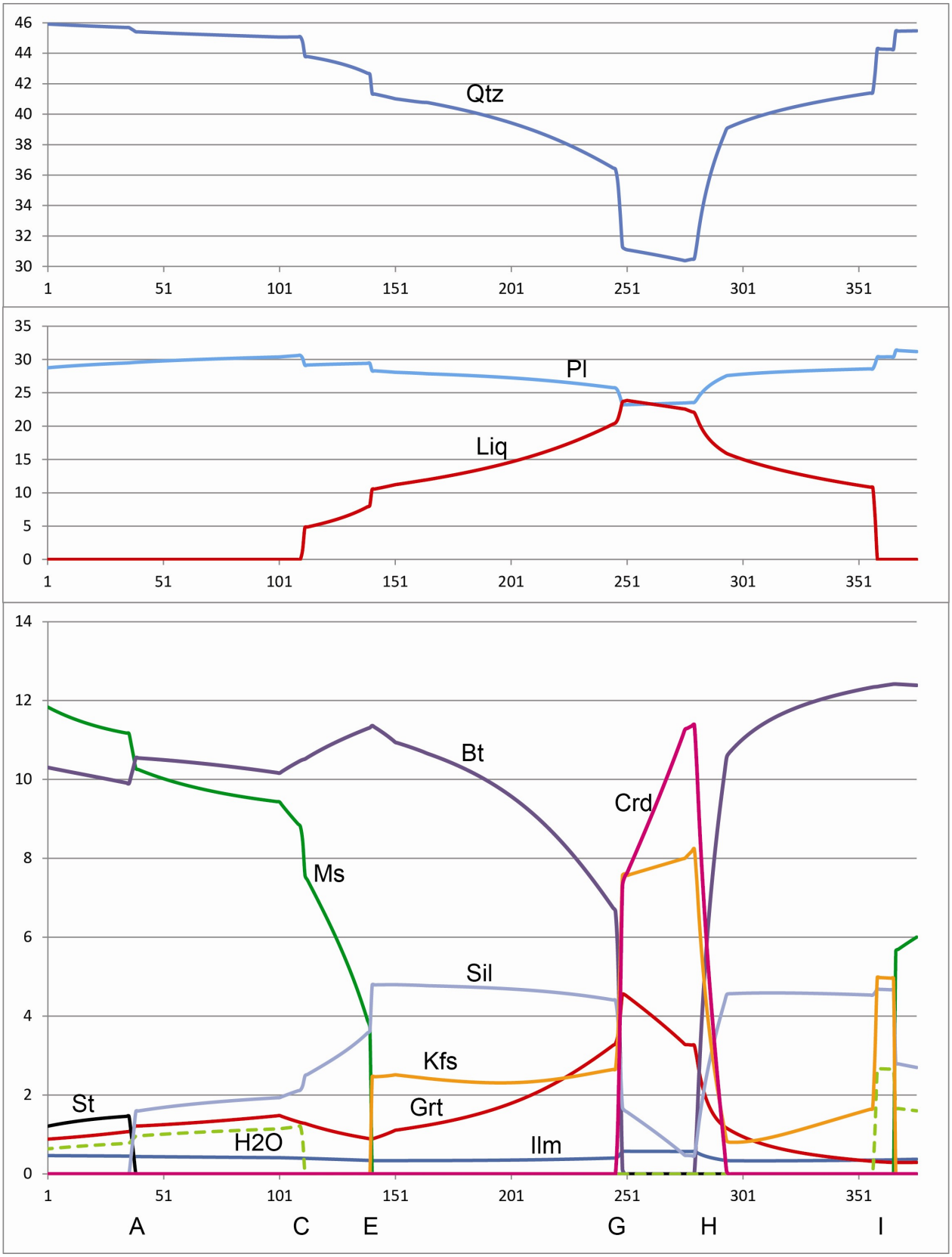

Tidigare skrifter i serien "Examensarbeten i Geologi vid Lunds universitet":

279. Dyck, Brendan, 2011: A key fold structure within a Sveconorwegian eclogite-bearing deformation zone in Halland, south-western Sweden: geometry and tectonic implications. (45 hp)
280. Hansson, Anton, 2011: Torvstratigrafisk studie av en trädstamshorisont i Viss mosse, centrala Skåne kring 4 000 - 3 000 cal BP med avseende på klimat- och vattenståndsförändringar. (15 hp)
281. Åkesson, Christine, 2011: Vegetations-utvecklingen i nordvästra Europa under Eem och Weichsel, samt en fallstudie av en submorän, organisk avlagring i Bellinga stenbrott, Skåne. (15 hp)
282. Silveira, Eduardo M., 2011: First precise U-Pb ages of mafic dykes from the São Francisco Craton. (45 hp)
283. Holm, Johanna, 2011**:** Geofysisk utvärdering av grundvattenskydd mellan väg 11 och Vombs vattenverk. (15 hp)
284. Löfgren, Anneli, 2011: Undersökning av geofysiska metoders användbarhet vid kontroll av den omättade zonen i en infiltrationsdamm vid Vombverket. (15 hp)
285. Grenholm, Mikael, 2011: Petrology of Birimian granitoids in southern Ghana - petrography and petrogenesis. (15 hp)
286. Thorbergsson, Gunnlaugur, 2011: A sedimentological study on the formation of a hummocky moraine at Törnåkra in Småland, southern Sweden. (45 hp)
287. Lindskog, Anders, 2011: A Russian record of a Middle Ordovician meteorite shower: Extraterrestrial chromite in Volkhovian-Kundan (lower Darriwilian) strata at Lynna River, St. Petersburg region. (45 hp)
288. Gren, Johan, 2011: Dental histology of Cretaceous mosasaurs (Reptilia, Squamata): incremental growth lines in dentine and implications for tooth replacement. (45 hp)
289. Cederberg, Julia, 2011: U-Pb baddelyit dateringar av basiska gångar längs Romeleåsen i Skåne och deras påverkan av plastisk deformation i Protoginzonen (15 hp)
290. Ning, Wenxing, 2011: Testing the hypothesis of a link between Earth's magnetic field and climate change: a case study from southern Sweden focusing on the 1st millennium BC. (45 hp)
291. Holm Östergaard, Sören, 2011: Hydrogeology and groundwater regime of the Stanford Aquifer, South Africa. (45 hp)
292. Tebi, Magnus Asiboh, 2011: Metamorphosed and partially molten hydrothermal alteration zones of the Akulleq glacier area, Paamiut gold province, South-West Greenland. (45 hp)
293. Lewerentz, Alexander, 2011: Experimental zircon alteration and baddeleyite formation in silica saturated systems: implications for dating hydrothermal events. (45 hp)
294. Flodhammar, Ingrid, 2011: Lövestads åsar: En isälvsavlagring bildad vid inlandsisens kant i Weichsels slutskede. (15 hp)
295. Liu, Tianzhuo, 2012: Exploring long-term trends in hypoxia (oxygen depletion) in Western Gotland Basin, the Baltic Sea. (45 hp)
296. Samer, Bou Daher, 2012: Lithofacies analysis and heterogeneity study of the subsurface Rhaetian–Pliensbachian sequence in SW Skåne and Denmark. (45 hp)
297. Riebe, My, 2012: Cosmic ray tracks in chondritic material with focus on silicate mineral inclusions in chromite. (45 hp)
298. Hjulström, Joakim, 2012: Återfyllning av borrhål i geoenergisystem: konventioner, metod och material. (15 hp)
299. Letellier, Mattias, 2012: A practical assessment of frequency electromagnetic inversion in a near surface geological environment. (15 hp)
300. Lindenbaum, Johan, 2012: Identification of sources of ammonium in groundwater using stable nitrogen and boron isotopes in Nam Du, Hanoi. (45 hp)
301. Andersson, Josefin, 2012: Karaktärisering av arsenikförorening i matjordsprofiler kring Klippans Läderfabrik. (45 hp)
302. Lumetzberger, Mikael, 2012: Hydrogeologisk kartläggning av infiltrationsvattentransport genom resistivitetsmätningar. (15 hp)
303. Martin, Ellinor, 2012: Fossil pigments and pigment organelles – colouration in deep time. (15 hp)

304. Rådman, Johan, 2012: Sällsynta jordartsmetaller i tungsand vid Haväng på Österlen. (15 hp)
305. Karlstedt, Filippa, 2012: Jämförande geokemisk studie med portabel XRF av obehandlade och sågade ytor, samt pulver av Karlshamnsdiabas. (15 hp)
306. Lundberg, Frans, 2012: Den senkambriska alunskiffern i Västergötland – utbredning, mäktigheter och faciestyper. (15 hp)
307. Thulin Olander, Henric, 2012: Hydrogeologisk kartering av grundvattenmagasinet Ekenäs-Kvarndammen, Jönköpings län. (15 hp)
308. Demirer, Kursad, 2012: U-Pb baddeleyite ages from mafic dyke swarms in Dharwar craton, India – links to an ancient supercontinent. (45 hp)
309. Leskelä, Jari, 2012: Loggning och återfyllning av borrhål – Praktiska försök och utveckling av täthetskontroll i fält. (15 hp)
310. Eriksson, Magnus, 2012: Stratigraphy, facies and depositional history of the Colonus Shale Trough, Skåne, southern Sweden. (45 hp)
311. Larsson, Amie, 2012: Kartläggning, beskrivning och analys av Kalmar läns regionalt viktiga vattenresurser. (15 hp)
312. Olsson, Håkan, 2012: Prediction of the degree of thermal breakdown of limestone: A case study of the Upper Ordovician Boda Limestone, Siljan district, central Sweden. (45 hp)
313. Kampmann, Tobias Christoph, 2012: U-Pb geochronology and paleomagnetism of the Westerberg sill, Kaapvaal Craton – support for a coherent Kaapvaal-Pilbara block (Vaalbara). (45 hp)
314. Eliasson, Isabelle Timms, 2012: Arsenik: förekomst, miljö och hälsoeffekter. (15 hp)
315. Badawy, Ahmed Salah, 2012: Sequence stratigraphy, palynology and biostratigraphy across the Ordovician-Silurian boundary in the Röstånga-1 core, southern Sweden. (45 hp)
316. Knut, Anna, 2012: Resistivitets- och IP-mätningar på Flishultsdeponin för lokalisering av grundvattenytor. (15 hp)
317. Nylén, Fredrik, 2012: Förädling av ballastmaterial med hydrocyklon, ett fungerande alternativ? (15 hp)
318. Younes, Hani, 2012: Carbon isotope chemostratigraphy of the Late Silurian Lau Event, Gotland, Sweden. (45 hp)
319. Weibull, David, 2012: Subsurface geological setting in the Skagerrak area – suitability for storage of carbon dioxide. (15 hp)
320. Petersson, Albin, 2012: Förutsättningar för geoenergi till idrottsanläggningar i Kallerstad, Linköpings kommun: En förstudie. (15 hp)
321. Axbom, Jonna, 2012: Klimatets och människans inverkan på tallens etablering på sydsvenska mossar under de senaste århundradena – en dendrokronologisk och torvstratigrafisk analys av tre småländska mossar. (15 hp)
322. Kumar, Pardeep, 2012: Palynological investigation of coal-bearing deposits of the Thar Coal Field Sindh, Pakistan. (45 hp)
323. Gabrielsson, Johan, 2012: Havsisen i arktiska bassängen – nutid och framtid i ett globalt uppvärmningsperspektiv. (15 hp)
324. Lundgren, Linda, 2012: Variation in rock quality between metamorphic domains in the lower levels of the Eastern Segment, Sveconorwegian Province. (45 hp)
325. Härling, Jesper, 2012: The fossil wonders of the Silurian Eramosa Lagerstätte of Canada: the jawed polychaete faunas. (15 hp)
326. Qvarnström, Martin, 2012: An interpretation of oncoid mass-occurrence during the Late Silurian Lau Event, Gotland, Sweden. (15 hp)
327. Ulmius, Jan, 2013: P-T evolution of paragneisses and amphibolites from Romeleåsen, Scania, southernmost Sweden. (45 hp)

LUNDS UNIVERSITET

Geologiska institutionen
Lunds universitet
Sölvegatan 12, 223 62 Lund